Toward a unified chromatic induction model

Xavier Otazu
Computer Vision Center, Computer Science Department, Universitat Autònomade Barcelona, Cerdanyola del Vallès, Barcelona, Spain

C. Alejandro Parraga
Computer Vision Center, Computer Science Department, Universitat Autònomade Barcelona, Cerdanyola del Vallès, Barcelona, Spain

Maria Vanrell
Computer Vision Center, Computer Science Department, Universitat Autònomade Barcelona, Cerdanyola del Vallès, Barcelona, Spain

In a previous work (X. Otazu, M. Vanrell, & C. A. Párraga, 2008b), we showed how several brightness induction effects can be predicted using a simple multiresolution wavelet model (BIWaM). Here we present a new model for chromatic induction processes (termed Chromatic Induction Wavelet Model or CIWaM), which is also implemented on a multiresolution framework and based on similar assumptions related to the spatial frequency and the contrast surround energy of the stimulus. The CIWaM can be interpreted as a very simple extension of the BIWaM to the chromatic channels, which in our case are defined in the MacLeod–Boynton (*lsY*) color space. This new model allows us to unify both chromatic assimilation and chromatic contrast effects in a single mathematical formulation. The predictions of the CIWaM were tested by means of several color and brightness induction experiments, which showed an acceptable agreement between model predictions and psychophysical data.

Keywords: visual system, color induction, wavelet transform

Citation: Otazu, X., Parraga, C. A., & Vanrell, M. (2010). Toward a unified chromatic induction model. *Journal of Vision, 10*(12):5, 1–24, http://www.journalofvision.org/content/10/12/5, doi:10.1167/10.12.5.

Introduction

Chromatic induction refers to changes of color appearance that occur when an object is observed in the presence of other colored objects. Chromatic induction effects (long known to artists and scientists such as Chevreul, 1839; da Vinci, 1651/2005; and Helmholtz, 1867) can be quite dramatic, as in the case of "simultaneous color contrast", when colored objects are perceived to have brightness and hue complementary to those of their surroundings. These variations in visual aspect (which are strongly dependent on the context, highly non-linear, and consequently difficult to reduce to a simple mathematical formulation) are frequently simplified or ignored by computational models of color appearance (Fairchild, 1998). However, there are many cases where these effects are strong and should be accounted for in order to have a proper understanding of the visual world.

Early chromatic induction studies explored the changes in brightness and color using test spots or disks with homogeneous surrounds. They revealed that chromatic induction increases roughly with the size of the inducing area (Kinney, 1962; Kirschmann, 1890) and that it saturates when the inducing surround field reaches a diameter of about 2–3 deg (for a 1 deg test field; Walraven, 1973; Wässle & Heinrich, 1970). They also found that the effect decreases as the distance between test and inducing regions increases (Jameson & Hurvich, 1961; Kirschmann, 1890), reaching a minimum for separations beyond 1.5 deg (Wässle & Heinrich, 1970). These results were later confirmed by Chubb, Sperling, and Solomon (1989) and Singer and D'Zmura (1994) using inhomogeneous stimulus (a disk filled with binary noise). The later also found a lack of orientation selectivity (suggesting that chromatic induction is spatially isotropic), low-pass temporal characteristics, and strong interocular transfer (suggesting that there might be both retinal and cortical contributions to these phenomena). In the same work, Singer and D'Zmura, hypothesized that the effects might depend on the grain of the noise (i.e., the spatial frequency (SF) content of the inducer and test stimuli). Indeed, several early models (Chichilnisky & Wandell, 1995; Lucassen & Walraven, 1993; Valberg & Lange-Malecki, 1990) and studies (Brenner & Cornelissen, 1998; Ware & Cowan, 1982; Werner & Walraven, 1982) of color appearance simply reduced the problem of color contrast in complex surrounds to the less complicated (and better understood) problem of color contrast in (equivalent) uniform surrounds. However, more recent research (Brenner, Ruiz, Herraiz, Cornelissen,

doi: 10.1167/10.12.5 Received August 10, 2009; published October 5, 2010 ISSN 1534-7362

& Smeets, 2003; Brown & MacLeod, 1997; Harrar & Vienot, 2005; Monnier & Shevell, 2003; Shevell & Monnier, 2005; Shevell & Wei, 1998; Wesner & Shevell, 1992) has shown that the color appearance of a central patch depends not only on the average properties of the light coming from its surroundings but on the spatial distribution and the variability of these surround colors as well (more chromatic variability makes test surfaces look less saturated). These "gamut normalization" effects can be dissociated in both luminance and chromatic dimensions, suggesting the operation of processes at the level of these visual pathways (Brown & MacLeod, 1997; D'Zmura & Singer, 1999).

Further evidence on the effects of chromatic changes in remote fields (over 10 deg away from the fovea) upon the color appearance of a centrally fixated (1 deg) test field was presented by Wachtler, Albright, and Sejnowski (2001). According to these results, chromaticity changes in the remote field had virtually no inducing effect unless there was also a change in the (immediate) background color. The inducing effect of the remote field was estimated to be about 8% of that corresponding to the background color.

Modeling attempts

There have been many attempts to model induction phenomena. These are usually classified according to their emphasis on low-level features (such as the contrast sensitivity function or CSF), object integration features (such as in "filling-in" models), symbolic descriptions, etc. (for a review, see Gilchrist, 2006; Pessoa, 1996). We have already discussed some of these models' characteristics in a previous work (Otazu, Vanrell, & Párraga, 2008b), and therefore here we will concentrate only on the attributes that are relevant to our current model.

Earlier low-level modeling attempts of induction phenomena concentrated on pure brightness induction. There are some such models in the literature (Blakeslee & McCourt, 1999; Kingdom, 1999; Otazu et al., 2008b; Xing & Heeger, 2001), which account for some of these perceptual changes and can reproduce some well-known visual effects. Although there are chromatic induction models as well (Singer & D'Zmura, 1995; Spitzer & Barkan, 2005), the second phenomena is far less studied.

Following on their previous psychophysical work, Singer and D'Zmura (1994, 1995) proposed a model to predict the changes of appearance of a central area in the presence of colored surrounding areas, based on ideas first suggested by Chubb et al. (1989). In their model, neurons tuned to certain SF bands had their responses weighted more strongly by the responses of similarly SF-tuned and similarly oriented neurons (a classical multiresolution framework). These neurons were separated into three chromatic "channels," each with its activity linearly weighted by the activity of the other two channels (feed-forward multiplicative gain control; D'Zmura, 1998; D'Zmura & Singer, 1999). The same authors reported a failure of earlier "divisive normalization" (Heeger, 1992; Sperling, 1989) theoretical frameworks to fit their psychophysical data (D'Zmura & Singer, 1999).

More recently, Spitzer and Barkan (2005) proposed a computational model based on two chromatic adaptation mechanisms (representing the influence of surrounding color and surrounding contrast, and called first- and second-order mechanisms) modeled in three stages: retinal ganglion-type opponency; cortical-type double opponency, and a "perceived image" stage (which is basically an inverse transformation of the resulting representation into a standard color space). The effects of local and remote adaptation at the first and second stage levels were simulated by gain control mechanisms (implemented as a shift in the response curve). Their model qualitatively predicts various induction effects. In 2008, Monnier (2008; Monnier & Shevell, 2004) reported that standard definitions of chromatic induction do not describe S-cone patterned backgrounds. He also suggests that both simultaneous contrast and assimilation are different manifestations of the same underlying perceptual process. Furthermore, he adds that the SF content (i.e., the complexity) of the scenes is the variable that differentiates between them. Our work is in line with these.

The Brightness Induction Wavelet Model (BIWaM)

Our previous attempt at modeling induction focused exclusively on brightness and consisted on a low-level multiresolution wavelet model called BIWaM (Otazu, Vanrell, & Párraga, 2008a; Otazu et al., 2008b). Despite its lack of free parameters, the BIWaM was capable of reproducing several visual effects such as simultaneous contrast, the *White effect*, grating induction, the *Todorovic effect*, *Mach bands*, the *Chevreul effect*, and the *Adelson–Logvinenko tile effects*, along with other previously unexplained effects such as the *dungeon illusion* (Bressan, 2001), using a single set of parameters and only three basic assumptions. The BIWaM unified brightness contrast and assimilation effects, modeling them as a single perceptual process. Brightness contrast describes a shift of the test stimulus brightness away from its surroundings and brightness assimilation describes the opposite (the brightness of the test stimulus shifts toward that of its surroundings).

In the present work, we apply the same principles to the color domain, assuming the independence between opponent color channels. This is achieved by treating chromatic and achromatic channels separately and applying the model to each channel in a simplistic manner. The purpose of this paper is not to provide a complete model of chromatic induction (this would require our model to be properly calibrated and tested against many more examples) but to

show how our small set of assumptions, when applied *en masse*, can have both good predictive and explanatory power.

The Chromatic Induction Wavelet Model (CIWaM)

The model we present here can be interpreted as a direct extension of the BIWaM into the color domain. While BIWaM works just on brightness, CIWaM applies the same basic principles simultaneously to brightness and the chromatically opponent visual pathways.

In what follows, we recall the three basic assumptions that form the basis of BIWaM, redefined here to include the chromatic case.

Assumption 1: spatial frequency. The induction effect operating on a stimulus of a particular SF in a given chromatic or achromatic channel is determined by the characteristics of its surround stimuli with the same SF (within an octave).

Assumption 2: spatial orientation. Assimilation in a given chromatic or achromatic channel is stronger when both the central stimulus and the surround stimulus have similar orientations. The opposite occurs for contrast effects. Consequently, when relative spatial orientation between stimulus and surround is orthogonal, assimilation of the central stimulus is the weakest and contrast is the strongest.

Assumption 3: surround contrast energy. Assimilation in a given chromatic or achromatic channel increases when the contrast energy of the surrounding features increases. Conversely, the contrast effect decreases when surround contrast energy increases.

The spatial frequency content of the surroundings is one of the main contributors to perceived changes of a central stimulus. In the particular case of brightness induction, several grating perception studies (Werner, 2003; Yu, Klein, & Levi, 2001, 2002) show that when the spatial frequencies of both central and surround stimuli are similar, brightness contrast of the central stimulus is reduced (brightness assimilation) and when these frequencies are different the central stimulus contrast is enhanced (brightness contrast). Therefore, brightness assimilation only occurs when both central and surround stimuli have similar spatial frequencies within a frequency range of about an octave (Blakemore & Campbell, 1969; De Valois, Albrecht, & Thorell, 1982; D'Zmura & Singer, 1999; Graham & Nachmias, 1971; Werner, 2003; Wilson, McFarlane, & Phillips, 1983; Yu et al., 2001, 2002). In our case, as a consequence of Assumptions 1 and 3, assimilation in a given chromatic or achromatic channel is stronger when both central and surround stimuli have similar spatial frequencies (within the one-octave bracket). Consequently, the opposite occurs for contrast effects, that is, contrast is strongest when spatial frequencies of a central stimulus and its surround are different.

Since this work is a straightforward extension of the BIWaM into the color domain, we use radially symmetric stimuli (see Methods section), without analyzing in detail the real impact of Assumption 2. Hence, the spatial variation related to this assumption is confined to just one dimension (i.e., the radial component of polar coordinates). Even though it is not analyzed here, Assumption 2 is supported by other research (Cannon & Fullenkamp, 1991; Solomon, Sperling, & Chubb, 1993; Yu et al., 2001, 2002; Yu, Klein, & Levi, 2003) and a more detailed study of the behavior of CIWaM with orientation will be done in the future.

Surround contrast is the third main contributor to chromatic induction as considered by our model. Its effects on a central stimulus (in the form of brightness assimilation effects) have been demonstrated by other researchers (Cannon & Fullenkamp, 1991; Chubb et al., 1989; Ejima & Takahashi, 1985; Ellemberg, Wilkinson, Wilson, & Arsenault, 1998; Klein, Stromeyer, & Ganz, 1974; MacKay, 1973; Nachmias & Sansbury, 1974; Yu et al., 2001, 2002, 2003).

The above assumptions rely on the relationship between induction effects and each specific spatial property, namely, SF, orientation, and surround contrast energy. In this new model, we suppose that induction effects occur separately in each pathway (the extent of this independence is currently not clear and has recently been challenged in the case of color shifts induced by S-cone patterns; Shevell & Monnier, 2006) and consequently, we propose a further assumption on how responses from the different pathways are combined to produce a final induction effect.

Assumption 4: channel independence and combination. The global induction effect at a given point is the result of the vector addition (in the chromatically opponent space) of the induction effects occurring independently in each color pathway.

As in the brightness-only version, Assumptions 1 and 2 are simulated using a multiresolution dyadic wavelet transformation. This transformation gives a new representation of the original image as a combination of a set of planes representing different frequencies and orientations, that is,

$$I = \sum_{s=1}^{n} (\omega_{s,h} + \omega_{s,d} + \omega_{s,v}) + c_n = \sum_{s=1}^{n} \sum_{o=h,d,v} \omega_{s,o} + c_n, \quad (1)$$

where I is the original image, $\omega_{s,o}$ are the given component images, also called wavelet planes, n represents different spatial frequencies, and c_n is the residual. Each plane contains the component of I with a given orientation o, at a specific spatial frequency s. Although

Assumption 2 is not tested here, we have used three different orientations, $o = h, v, d$ to represent 0, 90, and 45 degrees, respectively, to maintain consistency with our previous work.

The effects of assimilation and contrast explained in Assumptions 1 to 3 can be easily implemented by our model as a weighting function applied to the decomposed wavelet planes (and referred in this paper as α). This weighting function, which depends on two parameters, the spatial frequency of the plane considered and the ratio of contrast energy between each stimulus feature and its surrounds, allows us to recover the *perceived* or *induced* image I^p, from the decomposition of the original image (Equation 1). The resulting I^p is obtained by computing

$$I^p = \sum_{s=1}^{n} \sum_{0=v,h,d} \alpha_{s,r,o} \cdot \omega_{s,o} + c_n. \quad (2)$$

It is important to notice that $\alpha_{s,r,o}$, which modifies the coefficients obtained from the wavelet decomposition and is responsible for introducing the induction effects, is not a traditional weighting function, since its effects are dependent on the surrounding contrast acting on every single feature within each wavelet plane. As a consequence, for each pixel in the image, the weighting effects will act as stated by the Model Assumptions 1 to 3.

Up to this point, we have introduced the components of our new model that are similar to our previous brightness model (BIWaM) as described by Otazu et al. (2008b), particularly its key feature, the weighting function $\alpha_{s,r,o}$. Before we continue with the requirements for Assumption 4, we need first to review other ways in which this weighting function can be understood. Thus, in the next section we will attempt to provide a more thorough interpretation of $\alpha_{s,r,o}$, and following this, we will continue with our extension of the model to the color domain.

The weighting function or *extended CSF*

In the present model configuration, the weighting function, $\alpha_{s,r,o}$, is the main component responsible for most of the differences between the physical image and the output or *perceived* image. There are several constraints to $\alpha_{s,r,o}$. For start, we need to define a threshold SF value above which assimilation phenomenon overtakes contrast phenomenon (Smith, Jin, & Pokorny, 2001), with a shape resembling the well-known human CSF (Mullen, 1985) so that the CSF turns out to be a special case of the $\alpha_{s,r,o}$ when there is no center–surround energy unbalance (i.e., $r = 1$). We decided to name this function, *extended* CSF (or ECSF). Our previous work in brightness induction supported an ECSF that is low-pass when surround contrast energy is predominant and becomes band-pass when center contrast energy is predominant (Otazu et al., 2008b). For this reason, we decided to reformulate the weighting function that forms the core of BIWaM, generalizing it to include color phenomena. In the present analysis, we will assume that $\alpha_{s,r,o}$ depends on just two variables: the center–surround contrast energy ratio r and the spatial frequency s. Given that we did not test the real implications of Assumption 2, here we will suppose that the ECSF is independent of spatial orientation (its dependency of spatial orientation will be studied in detail in the future).

Since spatial frequency is linked to the geometry of the observational process, we will express s in terms of the stimulus visual angle and denote it as ν (in cycles per degree). The function we have selected for our model is displayed in Figure 1 (top panel), where the values of α are shown in terms of r and ν, that is $\alpha(\nu, r)$.

Considering particular values for the center–surround contrast energy ratio r, we can generate a family of weighting functions across all spatial frequencies, as shown in Figure 1 (bottom panel).

It is important to note here that the dependency of our proposed ECSF on the center–surround contrast energy ratio implies a variable CSF, since r varies at each point in the image. This newly introduced concept of a spatially variant CSF needs to be studied in more detail if we aspire to accurately model complex chromatic induction processes, since additional studies may reveal dependency on other factors such as overall scene intensity, the interaction between chromatic and achromatic channels, temporal adaptation, etc. However, as a first approximation, we will adopt an ECSF similar to the weighting function described previously (Otazu et al., 2008b).

Following the above, the weighting function (shown in Figure 1) that is at the core of our model can be written as

$$\alpha(\upsilon, r) = \begin{cases} \dfrac{r^2}{1+r^2} \exp\left(-\dfrac{\left(\log_2 \dfrac{4}{\upsilon}\right)^2}{2\sigma_1^2} \right) + \alpha_{\min}, & \upsilon \geq \upsilon_0; \\ \dfrac{r^2}{1+r^2} \exp\left(-\dfrac{\left(\log_2 \dfrac{4}{\upsilon}\right)^2}{2\sigma_2^2} \right) + \alpha_{\min}, & \text{otherwise} \end{cases}; \quad (3)$$

with

$$\alpha_{\min}(\upsilon, r) = \begin{cases} \exp\left(-\dfrac{\left(\log_2 \dfrac{4}{\upsilon}\right)^2}{2\sigma_3^2} \right), & \upsilon \geq \upsilon_0/4; \\ 1, & \text{otherwise}; \end{cases} \quad (4)$$

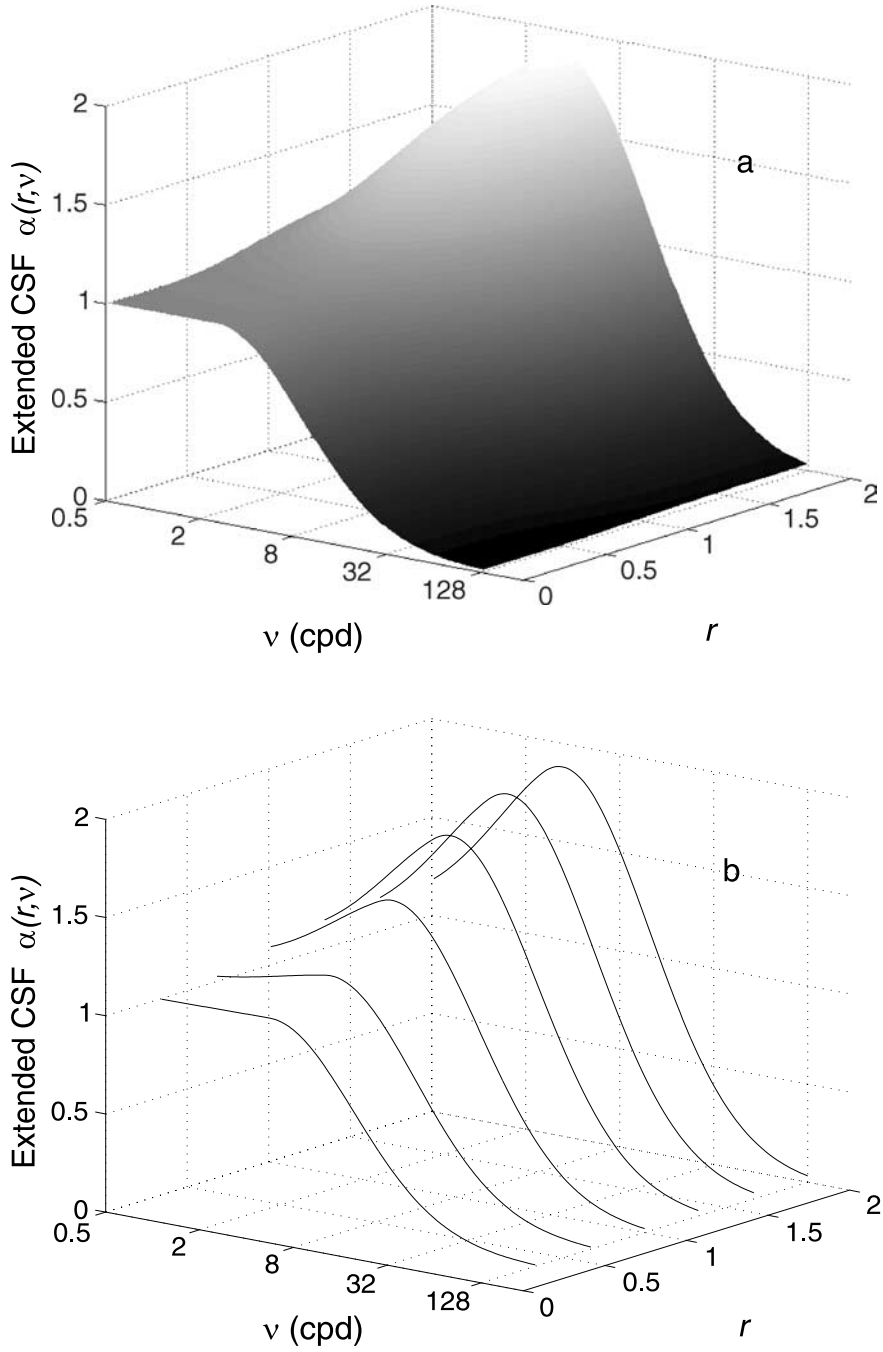

Figure 1. (Top) Graphical representation of the ECSF ($\alpha_{s,o,i}(r, \upsilon)$) for the luminance channel. (Bottom) Some profiles of the same surface along the SF (υ) axis for different center–surround contrast energy ratio values (r). The psychophysically measured CSF is a particular case of this family of curves (concretely for $r = 1$).

where $\upsilon_0 = 4$ cpd was adopted for the *luminance* channel and $\upsilon_0 = 2$ cpd for the *red–green* and *blue–yellow* chromatic channels according to psychophysical measures of both the peak of the human CSF (Mullen, 1985) and the transition point between assimilation and contrast (Fach & Sharpe, 1986; Simpson & McFadden, 2005; Smith et al., 2001; Walker, 1978). Both σ_2 and σ_3 were set to 1.25 and 2, respectively. To simulate the band-pass profile of the intensity channel's CSF and the low-pass profile of chromatic channels' CSF (Mullen, 1985), we set $\sigma_1 = 1.25$ for the luminance channel, and $\sigma_1 = 2$ for both the *red–green* and *blue–yellow* chromatically opponent channels.

In Figure 1, we show the profile of $\alpha(\nu, r)$ for the luminance channel. To avoid $\alpha(\nu, r)$ becoming null at low spatial frequencies, we introduced the term $\alpha_{\min}(\nu, r)$

so that $\alpha(\nu, r) \rightarrow \alpha_{min}(\nu, r)$ when $r \rightarrow 0$. This avoids a high degree of assimilation being performed at low SF (i.e., large-scale features), which would make parts of the image to reach zero value. Similarly, $\alpha_{min}(\nu, r) \rightarrow 1$ when $\nu \ll \nu_0$ (i.e., the lowest SFs), which implies $\alpha(\nu, r) \rightarrow 1$.

Color space

The space chosen to model chromatic induction processes is the cone excitation-based chromaticity space proposed by MacLeod and Boynton (which has three dimensions, namely l, s, and Υ, where the last represents luminance and is expressed in candelas per square meters; Boynton, 1986). This color space is based on a decomposition of the visual stimulus in three wavelength sensitive components (L, M, and S for long, middle, and short wavelengths as determined by Smith & Pokorny, 1975), which reflects the relative excitations of the human photoreceptors. It is also directly related to the physiology of the primate visual pathways and cortex in terms of postreceptoral color opponent signals, represented as orthogonal chromatic and achromatic axes (Derrington, Krauskopf, & Lennie, 1984).

Given that Assumption 4 reduces the CIWaM to a simple extension of the BIWaM to the chromatic domain, we applied the BIWaM to all l, s, and Υ channel representations of the original image in the MacLeod–Boynton space. In this context, the processing of the Υ channel by BIWaM is not different from the work already published (Otazu et al., 2008b). In the case of the l and s channels, we used a different ECSF (the same for both channels) because the spatial transfer characteristics of the chromatic channels are different from that of the achromatic channel (being the later band-pass in SF and the former low-pass; Mullen, 1985). At the moment, we make no distinction between the spatial transfer characteristics of the two chromatic channels. Whether a different mathematical expression should be used for each of the three color channels has to be determined in the future.

With the aim of testing the assumptions and the behavior of the CIWaM in general, we performed a series of psychophysical experiments and compared their results to corresponding model predictions. These are described in the next section.

Methods

Apparatus

All experiments were conducted on a 21″ CRT monitor (Viewsonic pf227f, "Trinitron" tube) viewed binocularly from a distance of 146 cm inside a dark room. The monitor was connected to an Nvidia Quadro FX3450/4000 SDI graphics card through a digital video processor (Cambridge Research Systems Bits++) capable of displaying 14-bit color depths at a 75-Hz (non-interlaced) rate. The system was gamma-corrected using a ColorCAL (Minolta) colorimeter. The full monitor screen contained 1280 × 1024 pixels, subtending some 15.5 × 11.5 deg to the observer. The controlling software was written in Matlab using Psychtoolbox (Brainard, 1997) and the Cambridge Research Systems custom-made toolbox to control the video processor. All chromaticities were specified in the cone-based opponent space of MacLeod and Boynton (Boynton, 1986), which is based in the Smith and Pokorny cone fundamentals (Smith & Pokorny, 1975). In this space, the abscissa l represents the "L vs. M" (or *red–green*) cone opponency and the ordinate s represents the "S vs. (L + M)" (or *blue–yellow*) cone opponency (where s is normalized to unity *equal-energy* white). The scaling of the s-axis in the MacLeod–Boynton space is essentially arbitrary (Boynton, 1986). However, we believe this does not impact on the generality of our results since CIWaM is based on a multiresolution computation that does not operate directly on absolute values (e.g., cone activations or luminance) but on dimensionless magnitudes such as contrast energy, which are always calculated relative to their surroundings.

Stimuli

We built our experimental stimuli (designed to measure changes in color appearance caused by a patterned background by means of an asymmetric color matching paradigm) following the work of Monnier and Shevell (2003, 2004; Shevell & Monnier, 2005). It consisted of a set of two circularly symmetric patterns (stimuli) presented side by side and separated 7.6 deg of visual angle from the observer's viewpoint on a dark background. The left side stimulus (namely the *reference stimulus*) consisted of a series of concentric rings alternating between two chromaticities with an extra ring of similar width (namely the *reference ring*) as shown in Figure 2. For the reader who is familiar with the experiments of Monnier and Shevell (to which the present experiments are closely related), we want to stress that the naming convention for "test" and "reference" (or "comparison") rings adopted here is opposite to theirs.

The two rings with alternating chromaticities are referred to as 1st and 2nd *inducers*, according to their physical proximity to the test ring. When the two inducers were chosen to have the same chromaticity, they formed a uniform chromatic background. The right side stimulus (the *test stimulus*) always consisted of a *test ring* (same size as the reference ring) placed over a uniform achromatic background approximately metameric to equal-energy white ($l = 0.66$, $s = 0.98$, $\Upsilon = 27.5$; Boynton,

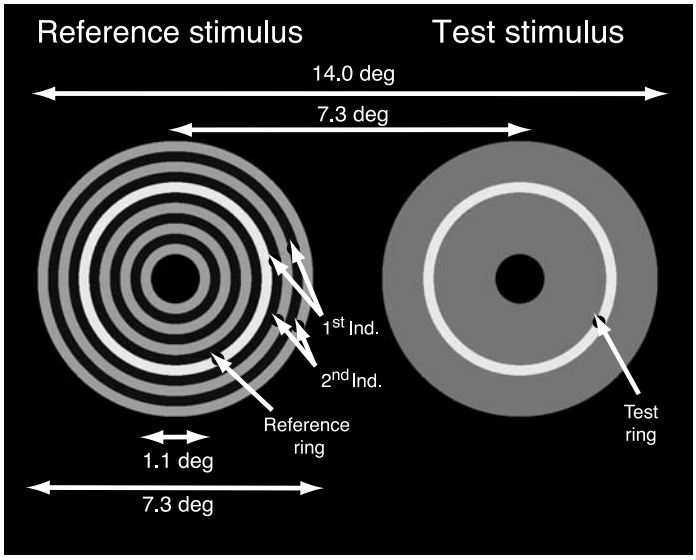

Figure 2. Schematics of the stimulus display. The number of annuli of the reference stimulus (in the example there are 11) varied between conditions. Subjects had to adjust the chromaticity and brightness of the *test ring* to match that of the *reference ring*.

1996; Monnier & Shevell, 2004). Both the chromaticities of the reference and inducer rings and the number of annuli on the reference stimulus were determined for each experimental condition according to Table 1. The chromaticities (in the MacLeod–Boynton space) corresponding to these conditions are shown in Figures 3 and 4.

We chose this rather limited number of conditions because here we just want to test the general behavior of BIWaM when extended to the color domain. A more comprehensive and detailed analysis to accurately and independently test each of the model's assumptions under many more conditions will be done in the future. For generality's sake, here we added a slight amount of luminance contrast to the stimuli (see Table 1). However, this luminance shift was kept small to stop it from becoming the dominant feature.

Experimental procedure

There were two *experiments* with three different *spatial configurations* consisting of rings of different widths each. The rings' widths were obtained by diving the reference stimulus width (see Figure 2) in 5, 11, or 17 parts. These spatial configurations of rings are subsequently referred as conf1, conf2, and conf3. The spatial frequencies of each of these configurations are 0.81, 1.77, and 2.74 cpd, respectively. The stimulus rings were rendered using four sets of colored patterns (also referred as *conditions*: see details in Table 1).

The test and inducer rings' sizes and colors were selected with the broad aim of maximizing induction effects and testing the assumptions in a more generalist way, but their choice was ultimately arbitrary.

In the first experiment, the two inducer rings had different chromaticities and luminances (see Table 1 and Figures 4 and 5), and in the second experiment, they had the same chromaticity and luminance (see Table 1 and Figures 3 and 7), resulting in a uniformly colored background.

Both experiments consisted of 12 runs (3 configurations × 4 conditions) and each session (consisting of Experiments 1 and 2) took between 40 and 50 min, depending on the observer's experience. The experiments were conducted in sequence, but the conditions and configurations were randomized. Observers had 2 min of dark adaptation and

	Reference ring			1st inducer			2nd inducer		
Conditions	*l*	*s*	ϒ	*l*	*s*	ϒ	*l*	*s*	ϒ
				Experiment 1 (striped background)					
1	0.66	0.98	27.5	0.64	1.40	20.0	0.68	0.60	37.0
2	0.67	1.00	26.0	0.64	1.40	20.0	0.64	0.60	32.0
3	0.66	0.98	27.5	0.68	1.40	22.0	0.64	0.60	32.0
4	0.65	1.00	30.0	0.68	1.40	22.0	0.68	0.60	37.0
				Experiment 2 (uniform background)					
1	0.64	1.00	26.0	0.64	0.60	32.0	0.64	0.60	32.0
2	0.66	0.60	34.5	0.68	0.60	37.0	0.68	0.60	37.0
3	0.68	1.00	29.5	0.68	1.40	22.0	0.68	1.40	22.0
4	0.66	1.40	21.0	0.64	1.40	20.0	0.64	1.40	20.0

Table 1. Summary of experiments and conditions (chromaticity sets). These chromaticities were applied to all spatial configurations (i.e., 5, 11, and 17 rings per disk). To see a plot of these values in the MacLeod–Boynton space, see Figure 3.

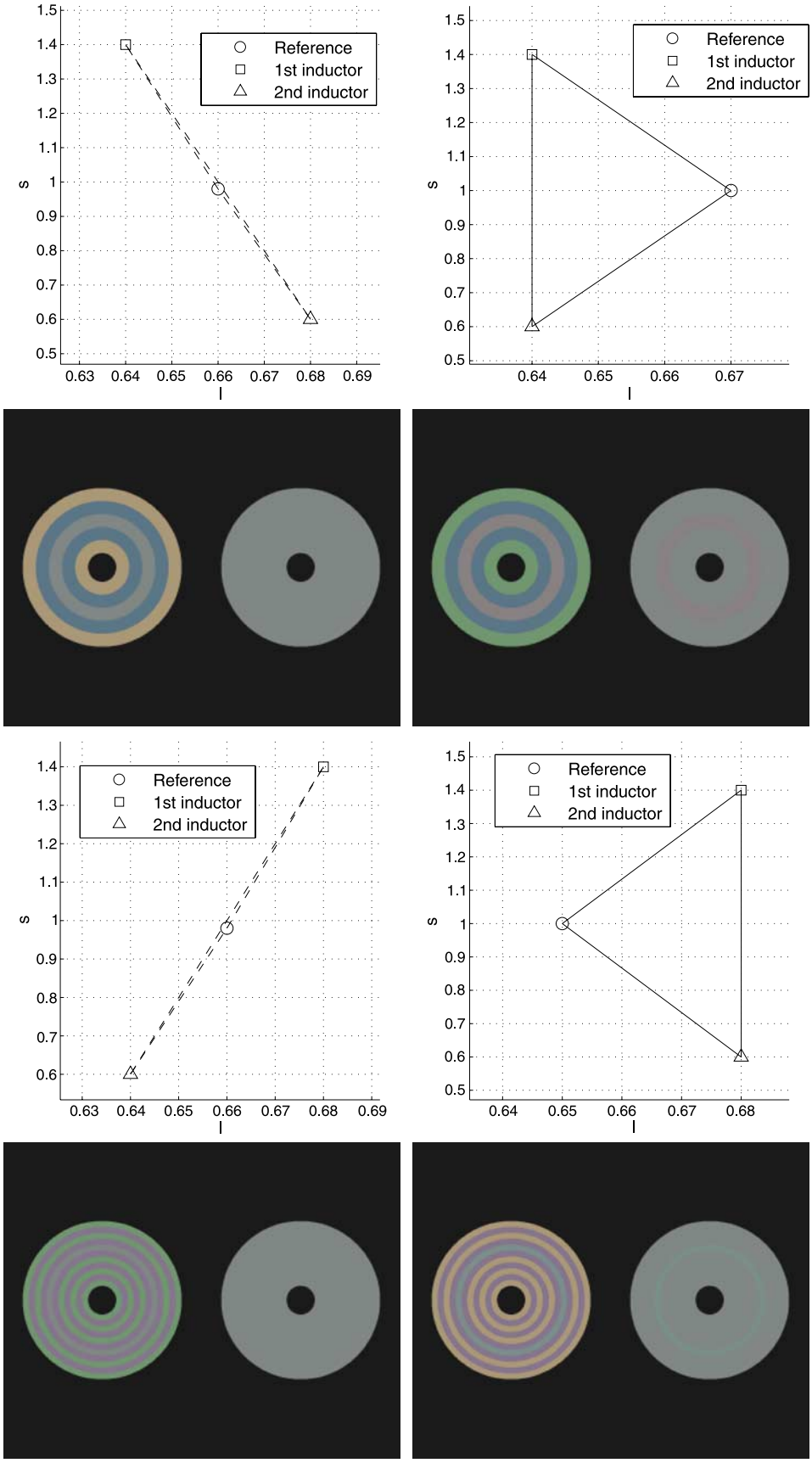

Figure 3. Experiment 2: position of the reference and inducer rings in the *I* vs. *s* chromaticity plane (1st and 2nd inducer chromaticity values are coincident). The symmetrical position of the colors was arbitrary and ϒ values were not the same (see Table 1 for details).

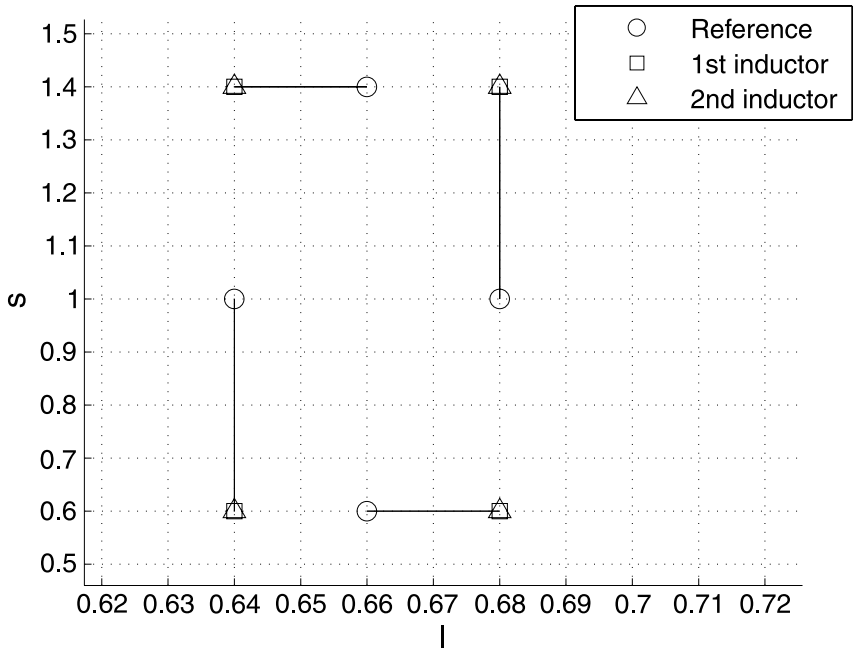

Figure 4. Examples of spatial configurations and conditions for Experiment 1. The plots show the position of the *reference* and 1st and 2nd inducer rings in the *l* vs. *s* chromaticity plane. The reference color, when represented in such plots, was always in a vertex, equidistant from the two inducer colors. For details of all chromaticity values, see Table 1.

their task was to match the appearance of the test ring to that of the reference ring by means of a Logitech gamepad connected to the PC. The controller buttons were programmed so that observers could navigate along each axis of the $ls\Upsilon$ MacLeod–Boynton cone space in an intuitive way (left = *greener*, right = *redder*, front = *bluer*, back = *yellower*, up = *lighter*, down = *darker*). There were no time constraints to the matching procedure and fixation was free with 10-s intervals between runs.

There were three main observers (two of the authors and one observer naive to the purposes of the experiment) who repeated the two experiments three times (in different days) and six other observers (five of them naive) who did the experiments only once. All the observers were staff or PhD students from our laboratory and were tested for normal color vision using the Ishihara and the Farnsworth Dichotomous (D-15) tests.

The images in Figure 4 show examples of the initial stimulus used in Experiment 1, considering several configurations (conf) and all four conditions (cond). In reading order: (conf1 cond1), (conf1 cond2), (conf2 cond3), (conf2 cond4).

For each run, the computer randomly selected an experiment/condition combination from the list (see Table 1) and assigned both the reference and test rings the same color and luminance, adding a 5% random jiggle to the test ring (in all three channels) to stop observers from memorizing key sequences. Although a 5% variation might represent a different amount of chromatic shift in each of the *l* and *s* chromatic axes (since the scaling of *s* is arbitrary), preliminary experiments showed that this amount was noticeable enough to serve the purpose of randomizing the starting point.

Since we were not interested in isolating any specific chromatic or luminance channel, but in testing the model's predictions in general (i.e., with the least possible number of constraints), the test and inducer rings were not isoluminant.

Results

To test the behavior of CIWaM, we performed two different analyses (each on both the psychophysical results and the CIWaM predictions).

Analysis 1: we computed the error of CIWaM (ideally zero) when it is applied to the psychophysical results obtained by the human observers. This reflects the fact that both sides of a color appearance asymmetric matching should be equivalent.

Analysis 2: we computationally simulated the psychophysical experiments. Here, the idea is to simulate a human observer (using CIWaM) performing a method-of-adjustment matching experiment, similar to what the real human observers did. This analysis allows us to find the physical color values that this simulated human (CIWaM observer) would impose on the test image in order to perceive it the same as the reference image. We also found

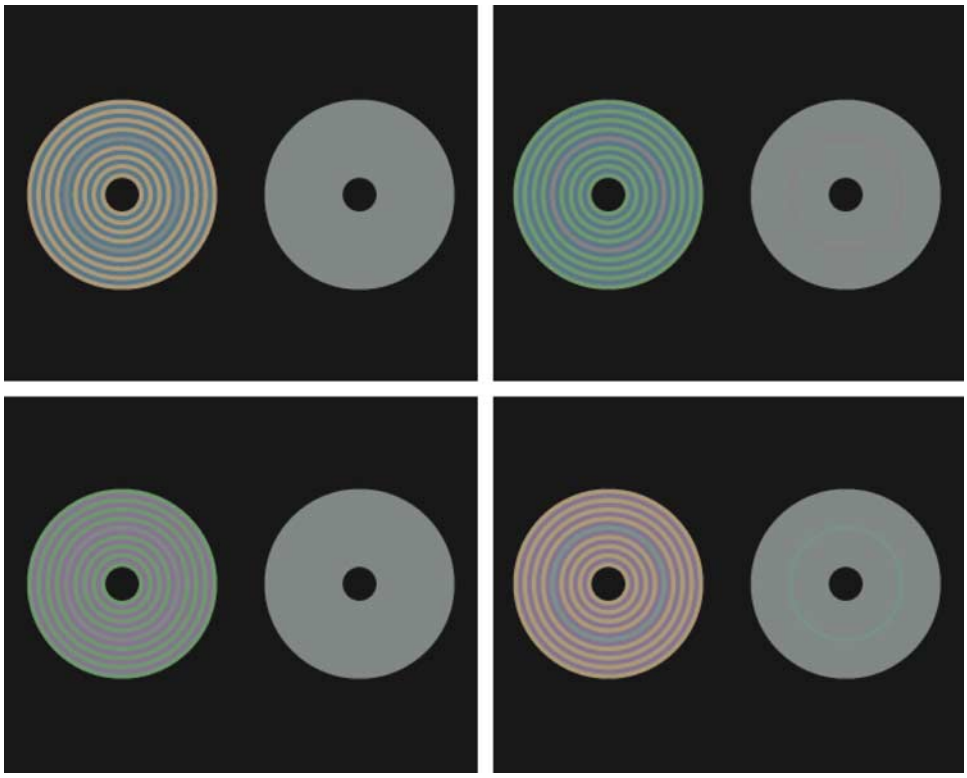

Figure 5. Examples of the initial stimulus used in Experiment 1. The chromaticity values of the 1st and 2nd inducers were different, and therefore, there was a series of concentric rings. One spatial configuration (17 rings) and all conditions (four color sets) are shown (see Table 1 for details).

Analysis 2 to be more convenient to explain in detail the workings of the model, and that is the main reason why it is included here.

Analysis 1: Perceptual reference–test difference

In the psychophysical experiments, observers modify the test ring color from its initial value $\mathbf{t}$ to its final value $\mathbf{t}_{\text{test}}$ so that its color is perceived the same as the reference ring's color $\mathbf{t}_{\text{ref}}$, e.g., $\mathbf{t}'_{\text{ref}} \cong \mathbf{t}'_{\text{test}}$, where $\mathbf{t}'_{\text{ref}}$ and $\mathbf{t}'_{\text{test}}$ are the perceived reference and test ring colors, respectively. To evaluate the accuracy of CIWaM, we apply it to the final image (obtained psychophysically), resulting in a CIWaM estimation of the colors perceived by the observers on both reference and test rings, i.e., $\mathbf{t}^{\text{CIWaM}}{}_{\text{ref}}$ and $\mathbf{t}^{\text{CIWaM}}{}_{\text{test}}$, respectively.

Since the psychophysical results $\mathbf{t}_{\text{test}}$ are distributed over the chromaticity plane, they have a standard deviation σ_{test} and correspondingly, the distribution of CIWaM-estimated values $\mathbf{t}^{\text{CIWaM}}{}_{\text{test}}$ has a corresponding standard deviation $\sigma^{\text{CIWaM}}{}_{\text{test}}$. In Figure 6, we show the average $\mathbf{t}^{\text{CIWaM}}{}_{\text{test}}$ values (colored void squares) with the corresponding error bars (standard deviation $\sigma^{\text{CIWaM}}{}_{\text{test}}$) alongside $\mathbf{t}^{\text{CIWaM}}{}_{\text{ref}}$ values (filled squares). Following the previous convention, colors of the reference and inducer rings (as detailed in Table 1 and Figure 4) are shown in empty black symbols. We also adopted a new convention regarding the three different configurations (as detailed in the Experimental procedure section): configuration 1 (or conf1) is always shown in red symbols, configuration 2 (or conf2) in blue symbols, and configuration 3 (or conf3) in green symbols.

If the CIWaM was 100% correct, we would obtain $\mathbf{t}^{\text{CIWaM}}{}_{\text{ref}} \cong \mathbf{t}^{\text{CIWaM}}{}_{\text{test}}$, that is, a zero difference between CIWaM-estimated colors for both the reference and test rings, hence filled and void squares in Figure 6 would coincide. In the Discussion section, we will analyze the correspondence of these two values.

Analysis 2: Computationally simulated experiments

In this second analysis, we simulated the psychophysical experiments within a computational framework. In this context, the model was set up to simulate the behavior of human observers, comparing the reference and test rings and adjusting the color of the second by small steps until both yielded similar outputs (i.e., reaches a stable solution). In this fashion, the final test ring colors obtained by the

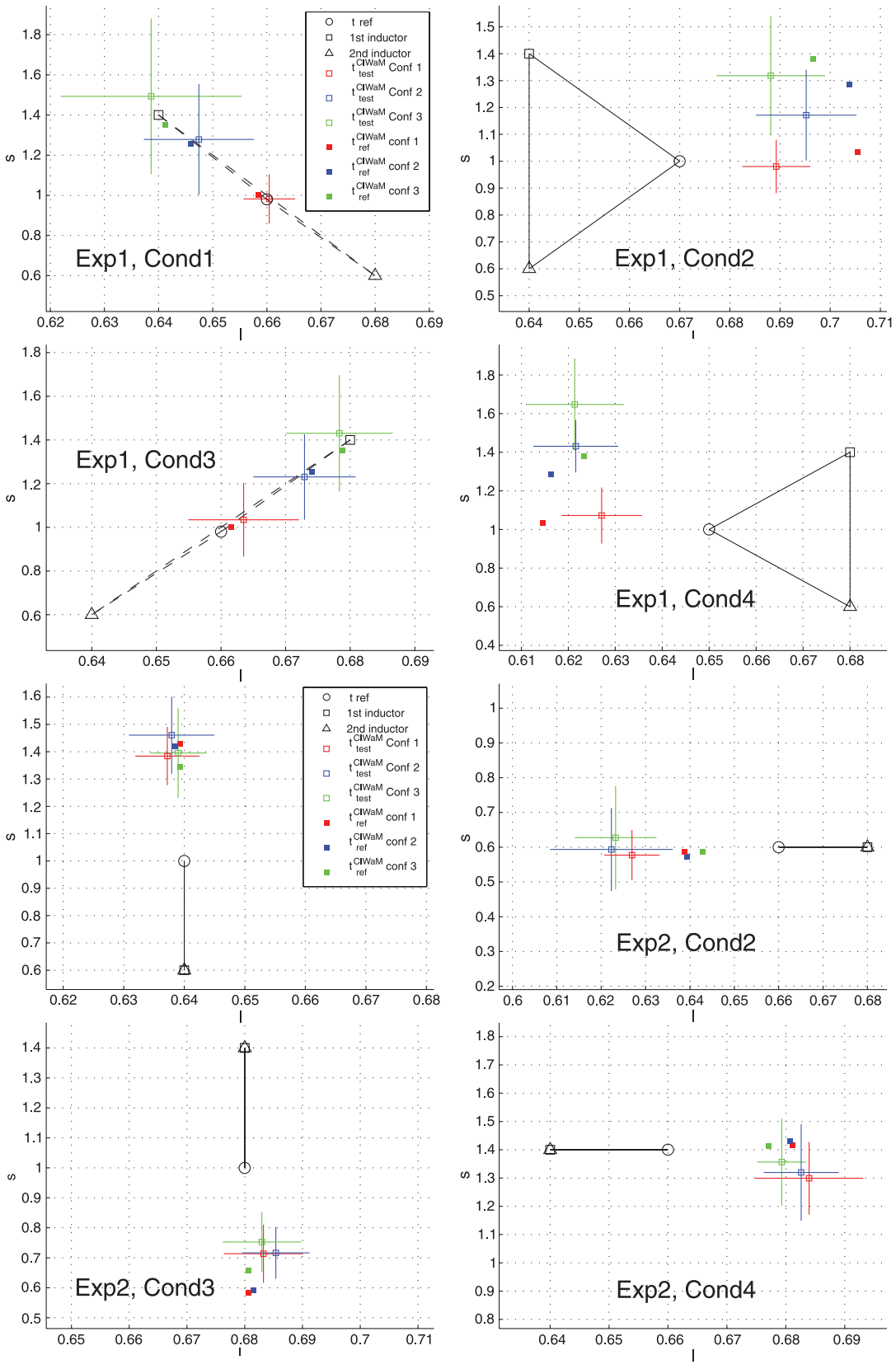

Figure 6. Average values of the CIWaM-estimated $\mathbf{t}^{CIWaM}_{test}$ (void squares) and $\mathbf{t}^{CIWaM}_{ref}$ (filled squares) for test and reference rings, respectively. Ideally, these values should be coincident. They are shown for every experiment, condition, and spatial configuration (red points for conf1, blue points for conf2, and green points for conf3). Lines are the associated standard deviation. The actual values for the psychophysical results are shown in Appendix A.

CIWaM observer can be compared to the final test ring colors obtained by the observers.

A single experimental run is simulated by the following iterative process:

1. Define test stimulus image I ($\mathbf{r}$ and $\mathbf{t}$ are the colors of the reference and test rings, respectively).
2. Use image I as input to CIWaM to obtain a simulated "perceived" image I_0.
3. From I_0 calculate the mean perceived colors $\mathbf{r}'$ and $\mathbf{t}'$ of the reference and test rings, respectively.
4. Calculate perceptual difference $\mathbf{d}' = \mathbf{r}' - \mathbf{t}'$, being $\mathbf{d}'$ the vector (d_l, d_s, d_Υ).
5. Define a new test ring color $\mathbf{t} = \mathbf{t} + 0.6 * \mathbf{d}'$.
6. If $d_l < \varepsilon_l$, $d_s < \varepsilon_s$, and $d_\Upsilon < \varepsilon_\Upsilon$, then return $\mathbf{t}_{\mathrm{CIWaM}} \equiv \mathbf{t}$ as the final value fitted else go to step 1.

A computationally simulated experiment run starts by taking the same initial reference and test ring colors $\mathbf{r}$ and $\mathbf{t}$ as the psychophysical experiment (see Methods section), i.e., the same initial stimulus image. From this input image, CIWaM observer obtains a "perceived" image from which we calculate the color difference between reference and test rings.

Since the final goal of the virtual experiment is to minimize this difference until the simulated observer perceive the two rings as equal, a small modification is applied in the direction of the "perceived change" (step 5, equivalent to the observer "pressing the gamepad button") and the iterative process is repeated. In order to stop the minimization process, we defined *a priori* three values (ε_l, ε_s, and ε_Υ), which are the maximum allowed difference between the perceived reference and test rings for each chromatic channel. When the differences are lower than these values, we consider that the rings are the same color and stop the iterations. In our particular case, we used $\varepsilon_l = 0.0001$, $\varepsilon_s = 0.001$, and $\varepsilon_\Upsilon = 0.05$ (Figure 7).

At the end of the iterative process, we obtain a simulated color $\mathbf{t}_{\mathrm{CIWaM}}$ for the test ring, which can be compared to the color $\mathbf{t}_{\mathrm{test}}$ obtained from the psychophysical experiments. We want to stress that in this notation the sub-index denotes the physical values obtained by the simulated CIWaM observer, whereas the super-index denotes the perceived values obtained by CIWaM.

CIWaM predictions and psychophysical results

The psychophysical results $\mathbf{t}_{\mathrm{test}}$ and their corresponding CIWaM observer predictions $\mathbf{t}_{\mathrm{CIWaM}}$ are displayed in Figures 8–10. We adopted the convention of showing

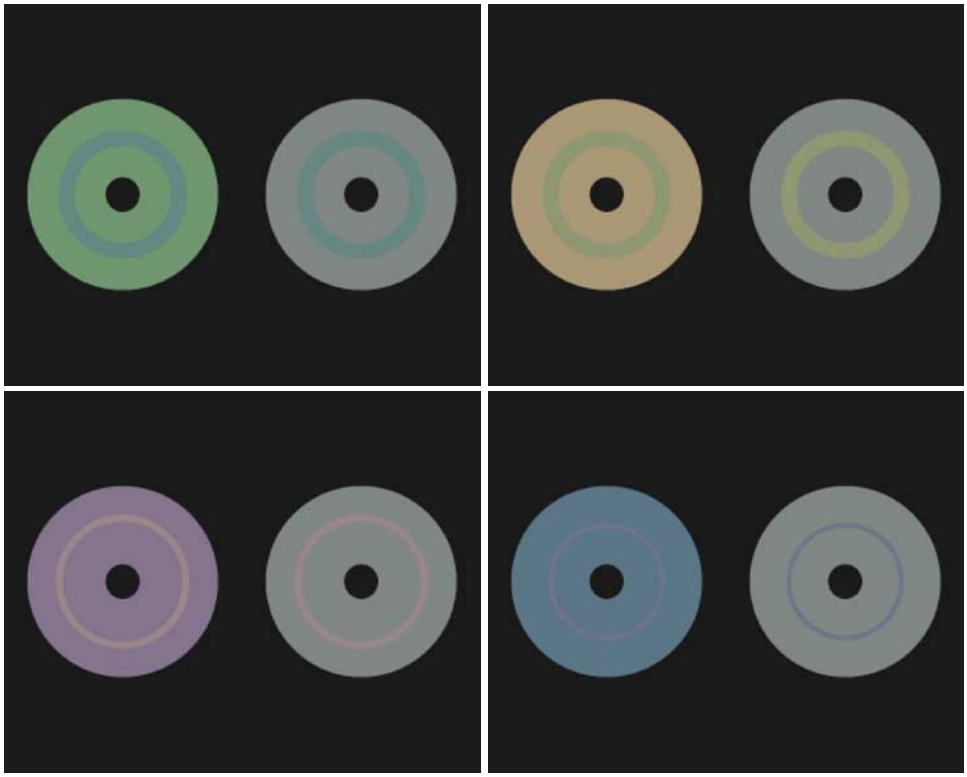

Figure 7. Examples of the initial stimulus used in Experiment 2. The chromaticity values of the 1st and 2nd inducers were the same, and therefore, the circular background is uniform. We show two spatial configurations (conf) and all four conditions (cond). In reading order, top: conf1, cond1; conf1, cond2; second row: conf2, cond3; conf3, cond4.

$\mathbf{t}_{CIWaM}$ as filled circles, with the empty circles indicating the results obtained by $\mathbf{t}_{test}$ (observers). The error bars on the plots show the standard deviation of our experimental results. In Figure 10, which shows several results in the same plot, we added arrows to illustrate which model prediction is connected to which experimental result.

Figure 8a shows the results obtained in Experiment 1, condition 1. On the top right panel, we can see that the psychophysical results $\mathbf{t}_{test}$ approximately lie on the diagonal line that joins the reference ring color (void black circle) with the two inducers (extremes of the diagonal line). CIWaM observer predicted values $\mathbf{t}_{CIWaM}$ also approximately lie on this diagonal line and they are close to the corresponding psychophysically obtained values for the three spatial configurations tested (shown in red, blue, and green symbols). In addition, the quantitative distribution of these points according to spatial configuration is similar, e.g., conf1 (5 stripes) results are higher on the *l*-axis and lower on the *s*-axis; conf3 (17 stripes) results are lower on the *l*-axis and higher on the *s*-axis, mimicking the psychophysics. A similar agreement also occurs in the Υ-axis (not shown, given that CIWaM is the same as the already tested BIWaM; Otazu et al., 2008b), confirming our hypothesis of independence between achromatic and chromatic channels.

In Figure 8b, we see that the CIWaM observer's predicted values for the final test ring color are in relative agreement with the psychophysical results. In addition, we notice an interesting effect that CIWaM also reproduces: in contrast to the example in Figure 8a, the final colors do not lie on the line joining the reference ring color and the first inducer color (this will be discussed in the next section). In Figures 9a and 9b, we see that the results for Cond3 and Cond4, respectively, retain the same attributes as expected, since the chromaticities in Figure 9a are symmetric to those of Figure 8a and the chromaticities in Figure 9b are symmetric to the ones in Figure 8b.

In Figure 10, we show the complete set of psychophysical results obtained from Experiment 2 and the corresponding CIWaM observer predictions. We can see that predictions and psychophysical results coincide in direction and magnitude. An interesting effect is that, as in the psychophysical experiment, CIWaM observer predictions are not aligned with the line joining the reference ring and inducer colors. We comment on the possible reasons for this in the next section.

Discussion

Analysis 1

As explained in the Results section, the experiment ended when observers perceive both reference and test rings as having the same color. The average standard deviation of these psychophysically determined test ring colors $\mathbf{t}_{test}$ is termed $\bar{\sigma}_{test}$ and includes all the experiments, configurations, and conditions shown in Table 2 (first row). When we apply CIWaM to each of the psychophysical solutions, we obtain a distribution of values with an average value $\mathbf{t}^{CIWaM}{}_{test}$, a standard deviation $\sigma^{CIWaM}{}_{test}$, and correspondingly, for each reference ring we obtain a value $\mathbf{t}^{CIWaM}{}_{ref}$ (with no standard deviation).

As mentioned before, if CIWaM was 100% correct its solution for both rings should be the same when applied to the observer-modified images (i.e., $\mathbf{t}^{CIWaM}{}_{ref} \cong \mathbf{t}^{CIWaM}{}_{test}$). The differences between the predicted values of the reference and test rings are the distances between a void square and its corresponding filled square in Figure 6.

To check for systematic errors, we plotted the values of $\mathbf{t}^{CIWaM}{}_{ref-test} = \mathbf{t}^{CIWaM}{}_{ref} - \mathbf{t}^{CIWaM}{}_{test}$ on the *ls* plane in Figure 11, which are distributed around (l, s, Υ) = (0, 0, 0), their ideal location. A similar distribution was obtained for the Υ channel. On the third row of Table 2, we show the standard deviation of the values plotted in Figure 11 ($\sigma^{CIWaM}{}_{ref-test}$), which can be interpreted as the error of CIWaM. In order to get an estimation of the significance of this error, the second row of Table 2 shows the mean standard deviation of observer responses ($\bar{\sigma}^{CIWaM}{}_{test}$) in all three channels. Table 2 allows us to compare the uncertainty of the model ($\sigma^{CIWaM}{}_{ref-test}$) to the uncertainty of the observer responses ($\bar{\sigma}^{CIWaM}{}_{test}$), showing that they are of similar magnitude.

In Figure 12, we show a general plot of the CIWaM-estimated reference ring color $\mathbf{t}^{CIWaM}{}_{ref}$ (abscissa) versus the CIWaM-estimated final test ring color $\mathbf{t}^{CIWaM}{}_{test}$ (ordinate) for all experiments, conditions, and subjects in each of the l, s, and Υ chromatic channels. There are 24 points in each plot (2 experiments × 3 configurations × 4 conditions). The dotted line (diagonal) is where all points should lie if CIWaM's predictions were 100% accurate.

The plots in Figure 12 show an approximately linear behavior, implying that the CIWaM predictions are qualitatively correct. The solid line represents the best fitting (linear regression), with slopes around 0.9 and correlation coefficients $c \cong 0.9$. The mean squares of the residuals r^2 is also shown for every channel in the figure.

Analysis 2

Predictions from the computationally simulated psychophysical experiment using CIWaM can be qualitatively interpreted by considering how the model operates on the information fed to each of its channels. To this aim, we have added, next to *l*- and *s*-axes of the central plots in Figures 8 and 13, the corresponding red–green and blue–yellow channel stimuli as "seen" by the model. In this section, we will analyze each experiment separately, with the aim of understanding more in detail the operation of the model.

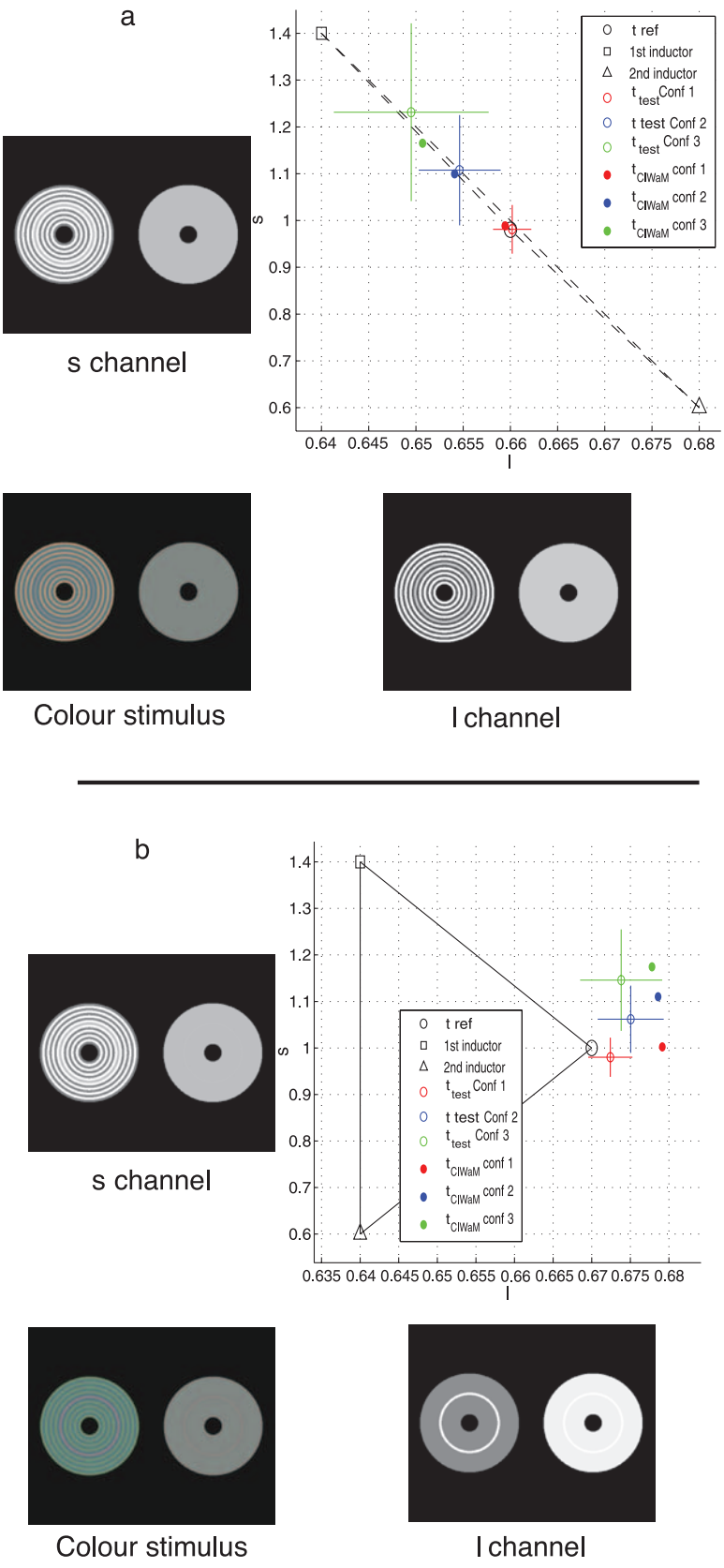

Figure 8. (a) Psychophysical results (void circles) and CIWaM predictions (filled circles) for Experiment 1, condition 1 in all three spatial configurations. (b) Psychophysical results (void circles) and CIWaM predictions (filled circles) for Experiment 1, condition 2 in all three spatial configurations (see text for explanation). Both panels: the bottom left picture shows the actual initial stimulus. Next to each chromatic axis we have added the corresponding channel image (only for conf3).

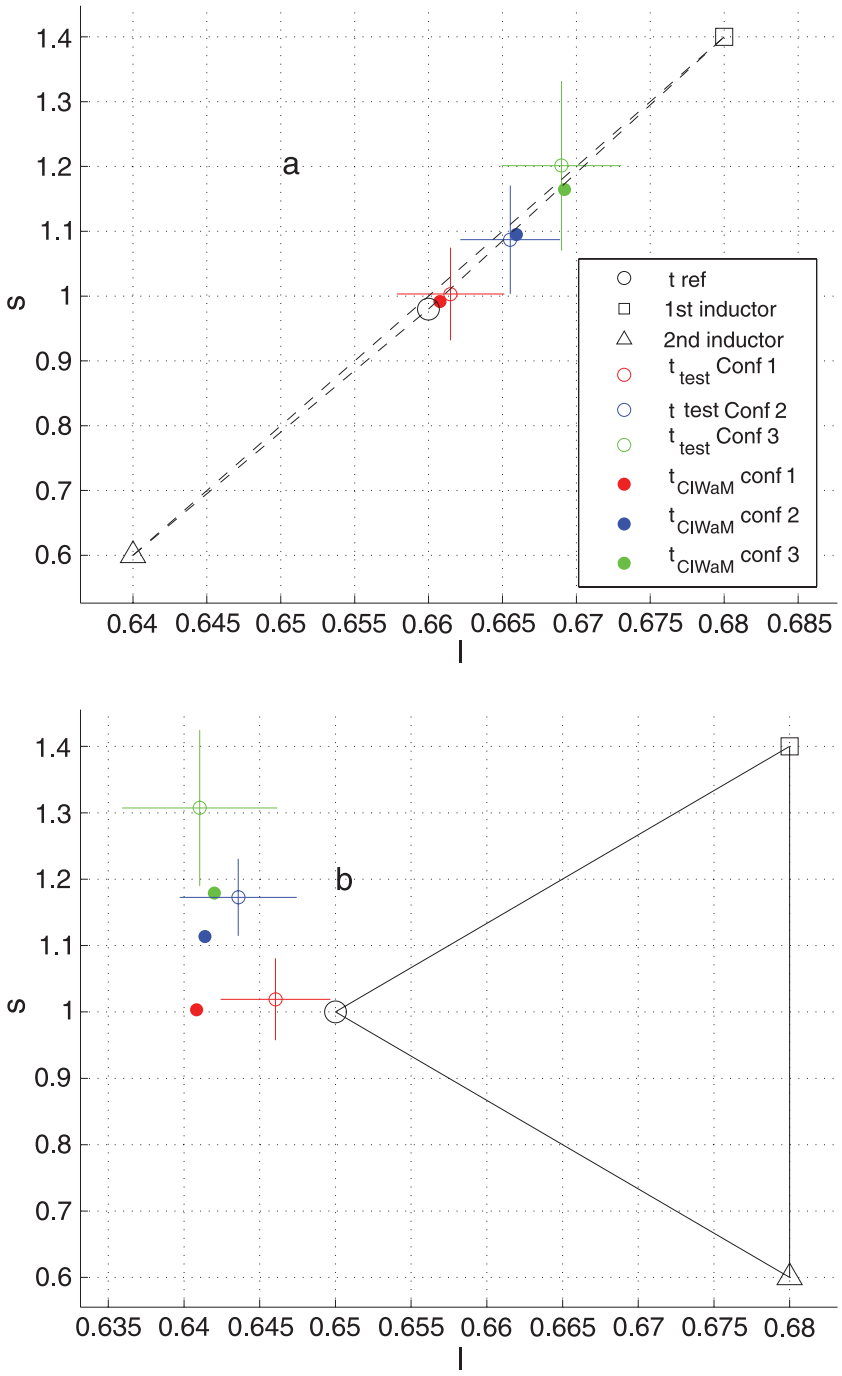

Figure 9. (a) Psychophysical (void circles) and CIWaM predictions (filled circles) for Experiment 1, condition 3 in all three spatial configurations. (b) Psychophysical (void circles) and CIWaM predictions (filled circles) for Experiment 1, condition 4 in all three spatial configurations.

Experiment 1

As shown in Figure 8a, both reference rings (the one seen by the model's l channel, and the one seen by the model's s channel) are surrounded by different sets of inducer rings (1st and 2nd inducers). The signals from these inducer rings are markedly different, implying relatively high surround contrast energy ($l_1 s_1 \Upsilon_1$ = [0.64, 1.40, 20.0]; $l_2 s_2 \Upsilon_2$ = [0.64, 1.40, 20.0]). For a complete list of chromaticity values, see Table 1.

By the model's *Assumption 3*, assimilation increases with increased surround contrast, i.e., the reference ring tends to the value of the 1st inducer ring in both the l and s channels. This is primarily the reason why both the psychophysical values (empty circles) and CIWaM predictions

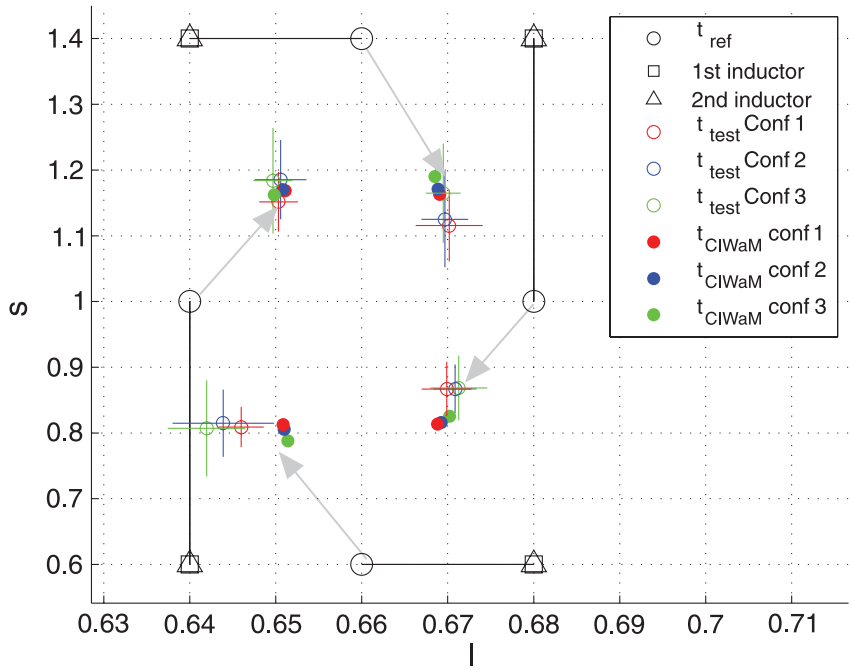

Figure 10. Experiment 2 (all conditions and configurations). The plot shows the chromaticity layout of both psychophysical results and CIWaM predictions for the second experiment. Both inducer colors were the same, forming a uniform circular background to the reference ring, hence squares and triangles are superimposed on the plot. Empty symbols represent psychophysics and filled symbols represent model predictions, while colors outline spatial configurations. The gray arrows relate each set of results to its corresponding reference and test colors.

(filled circles) lie along the diagonal that joins the reference ring and the first inducer ring colors: test ring chromatic values approach that of the 1st inducer.

The multiresolution wavelet algorithm decomposes the stimulus into one octave-bandwidth SF components, boosting or decreasing its contrast according to the ECSF (see Figure 1). That is, lower surround SFs yield lower assimilation/higher contrast and higher surround SFs yield the opposite. These effects are explained for the luminance case in Otazu et al. (2008b). Our results suggest that the rule governing chromatic induction processes is the same for both l and s channels. In Figure 8a, we can see that the assimilation effect is stronger or weaker depending on the ring's size and spatial configuration, being the lower SF result (conf1, red symbols) further away from the first inducer and the higher SF results (conf3, in green) closer along the diagonal. The dependency of these effects on spatial configuration is mainly because of the extended CSF behavior: a higher response on lower spatial frequencies (e.g., conf1, which implies lower assimilation and higher contrast) and a lower response on higher frequencies (e.g., conf3, which implies higher assimilation and lower contrast). Since these effects are applied simultaneously to both l and s channels using the same rule, the final result lies on the chromaticity diagonal.

There is another interesting effect that becomes apparent in Figure 8b. In this experiment, the results obtained by both the human observers and CIWaM observer do not lie on the line joining the reference ring color and the first inducer color. A priori we would expect the final test color to move toward the first inducer color (as in the previous condition) and the results to lie on the line joining these two colors. However, for all configurations, the results are shifted to the right of the test-inducer triangle, in the direction of the positive l channel. These results (and the model's behavior) were initially unexpected by the authors, who anticipated the colored points of the plot to be aligned toward the 1st inducer, not to be shifted toward the right side. However, it is possible to qualitatively explain these results again bearing in mind *Assumption 3*. In the s

	l	s	Υ
$\bar{\sigma}_{\text{test}}$	0.0037	0.0741	1.8846
$\bar{\sigma}^{\text{CIWaM}}{}_{\text{test}}$	0.0082	0.1633	4.3160
$\sigma^{\text{CIWaM}}{}_{\text{ref–test}}$	0.0077	0.0947	3.4563

Table 2. First row: mean standard deviation of the psychophysical results obtained by the observers for all the experiments, configurations, and conditions. Second row: mean standard deviation of $\mathbf{t}^{\text{CIWaM}}{}_{\text{test}}$ (see text for details). Third row: mean standard deviation of $\mathbf{t}^{\text{CIWaM}}{}_{\text{ref–test}}$ (as plotted in Figure 11—see text for details).

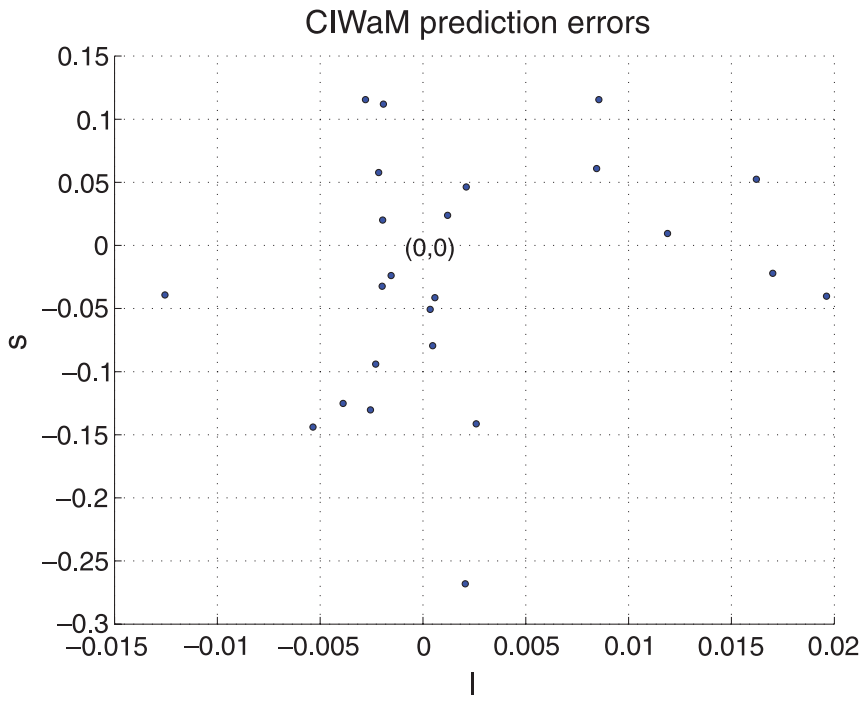

Figure 11. Distribution of $\mathbf{t}^{\mathrm{CIWaM}}{}_{\mathrm{ref-test}}$, which is a measure of CIWaM's inaccuracy (see text for details) on the *ls* chromatic plane. In the ideal case, all points should be on the (*l*, *s*) = (0, 0) location. See Table 2, third row for the standard deviation of this distribution.

chromatic channel, the reference ring has high surround contrast energy because of the different *s* values between the 1st and 2nd inducer rings. However, in the *l* chromatic channel, the first and second inducer rings have the same value, which means that the reference ring is on a uniform "*l*" background (see image next to the *l* channel). A uniform background on the *l* channel yields null surround contrast energy for the reference ring in that channel, which by means of *Assumption 3* implies that on the *l* channel contrast is high (i.e., it shifts away from the first inducer) and assimilation is low (i.e., it shifts toward the first inducer). Because of that, the *l* chromaticity value of the reference ring moves away from that of the first inducer (it has a higher *l* value). On the other hand, on the *s* channel the surround contrast energy is high, inducing assimilation (i.e., the reference–test rings move toward the 1st inducer). The combined effects on both channels is that the resulting reference ring chromaticity becomes higher on the *l* channel *and* on the *s* channel (i.e., it shifts toward the top right corner of the figure), which is different to what was expected from the previous results.

Similar results were obtained for experimental conditions 3 and 4 (shown in Figure 9) confirming the above interpretation of the results, given that these colors approximately mirror those of Figure 8 in the MacLeod–Boynton chromaticity diagram.

Experiment 2

In Figure 10, we show the results obtained by both CIWaM and the human observers for all chromatic conditions and configurations in a single plot. As with the previous results, they do not lie in the line joining the reference ring and the surround uniform inducer background. Since chromatic contrast is explained as the detachment of the test stimuli's chromaticity from that of its inducer, we would expect the final results to be located along this line, instead our results are shifted toward the center of the plot. Again, CIWaM approximately reproduces this effect and becomes a useful tool at explaining qualitatively the reason behind it. As discussed in the Results section, both the CIWaM and human observers change the test ring until it matches the reference ring. Chromatic induction from the inducer rings makes the reference ring to be perceived different than when it is viewed in isolation. However, the same type of induction modifies the appearance of the test ring (at the right, in Figure 2), that is surrounded by a uniform gray background, which in turn induces some kind of chromatic contrast on it. In a given experimental run, the observer changes the test ring color $\mathbf{t}_{\mathrm{test}}$ until the new perceived color $\mathbf{t}'_{\mathrm{test}}$ is equal to the color $\mathbf{t}'_{\mathrm{ref}}$ he perceives when observing the reference ring (color $\mathbf{t}_{\mathrm{ref}}$). Here both perceptual colors $\mathbf{t}'_{\mathrm{ref}}$ and $\mathbf{t}'_{\mathrm{test}}$ are influenced by their respective backgrounds. At the end of the run, we have $\mathbf{t}'_{\mathrm{test}} \cong \mathbf{t}'_{\mathrm{ref}}$.

Figure 13 shows an example of the final colors $\mathbf{t}_{\mathrm{test}}$ as obtained by both human observers (void colored circles with error bars) in condition 1 for all spatial configurations. These results are outside the reference–test line (as determined by the void black circle and square representing the reference–inducer background color). The shift induced by the colored uniform background on

the reference ring color $\mathbf{t}_{ref}$ as predicted by CIWaM observer is represented as a light blue dashed arrow ($\mathbf{t}'_{ref}$). However, it is when the induction effects of the gray uniform background on the test ring $\mathbf{t}_{test}$ are taken into account that a complete explanation emerges. In fact, CIWaM can perform an estimation of these perceptual $\mathbf{t}'_{test}$ and $\mathbf{t}'_{ref}$ colors. These are the $\mathbf{t}^{CIWaM}{}_{test}$ and $\mathbf{t}^{CIWaM}{}_{ref}$ values shown under the Analysis 1 heading in the Results section as filled squares in Figure 6.

The color difference between the uniformly gray background and the test ring $\mathbf{t}_{test}$ is represented in Figure 13 as a solid gray arrow. This color difference exerts the same effect on the test colors as the inducer–reference difference exerts in the reference colors: both arrows "push" their respective colors along their own axis and meet somewhere at the top. The color of the left ring $\mathbf{t}_{ref}$ shifts to become $\mathbf{t}'_{ref}$ and the color of the right ring $\mathbf{t}_{test}$ becomes $\mathbf{t}'_{test}$ where the subject sees them as equal, e.g., $\mathbf{t}'_{test} \cong \mathbf{t}'_{ref}$. The effect of the gray background is apparent from the psychophysical results and is also reproduced by CIWaM.

In Figure 14, we show the difference between the psychophysical results $\mathbf{t}_{test}$ and the CIWaM predictions $\mathbf{t}_{CIWaM}$ in the *ls* chromatic plane, i.e., $\mathbf{t}_{CIWaM-test} \equiv \mathbf{t}_{CIWaM} - \mathbf{t}_{test}$ (24 points: 2 experiments × 3 configurations × 4 conditions). We can see that they are randomly distributed around the ideal $\mathbf{t}_{CIWaM-test}$ = (0, 0, 0) and present a pattern similar to that of Figure 11 (again, we only show the *ls* chromatic plane to ease the visualization). In Table 3 (first row), we show the mean standard deviation of the psychophysical results ($\bar{\sigma}_{test}$) for all three *ls*ϒ channels. The second row shows the equivalent for the difference between model predictions and observers (the model's uncertainty, $\sigma_{CIWaM-test}$). These figures show that both are in good agreement. These results provide simple verification of Assumption 3 (influence of the surround contrast) in the model.

A comparison between both types of analysis is shown in Table 4, confirming that the uncertainty ratios of CIWaM and those of the observers are similar, independently of how the results are interpreted.

In Figure 15, we show a general plot of all predictions by CIWaM: $\mathbf{t}_{CIWaM}$ (abscissa) versus the psychophysical results $\mathbf{t}_{test}$ (ordinate) for all experiments, and configurations in each of the *l*, *s*, and ϒ chromatic channels. There are 24 points in each plot (2 experiments × 3 configurations × 4 conditions). Each point represents the mean value of a given experiment, condition, and configuration for all observers. The dotted line (diagonal) is where all points should lie if CIWaM's predictions were 100% accurate.

The plots show an approximately linear behavior, implying that the CIWaM predictions are qualitatively

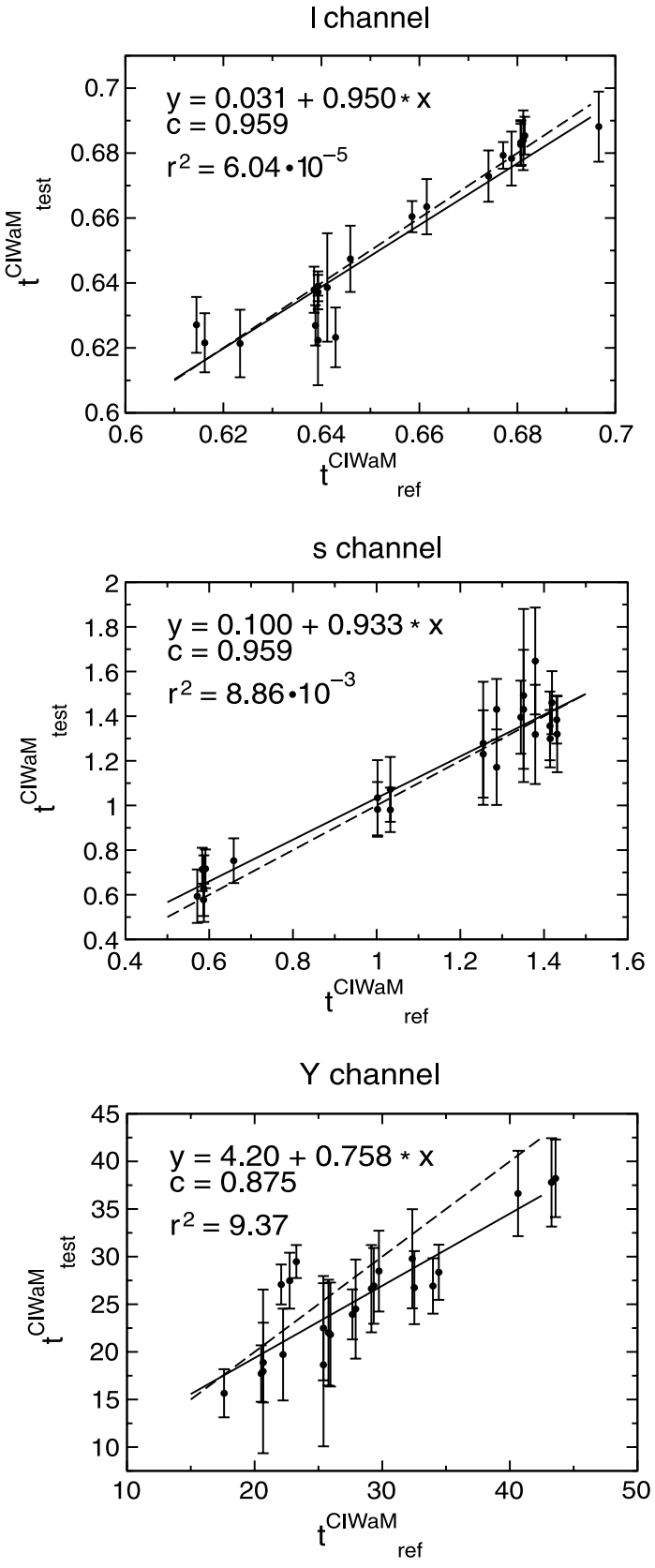

Figure 12. IWaM predicted perceptual colors for reference ring $\mathbf{t}^{CIWaM}{}_{ref}$ (abscissas) against test ring $\mathbf{t}^{CIWaM}{}_{test}$ (ordinates) for all the chromatic conditions and spatial configurations, separated according to MacLeod–Boynton chromaticity and luminance channel. Each point represents the color obtained by CIWaM for each one of both the reference and test ring color pair. The broken line shows the "unit" diagonal and the solid line shows the linear regression of the results. Details of the fits are also shown.

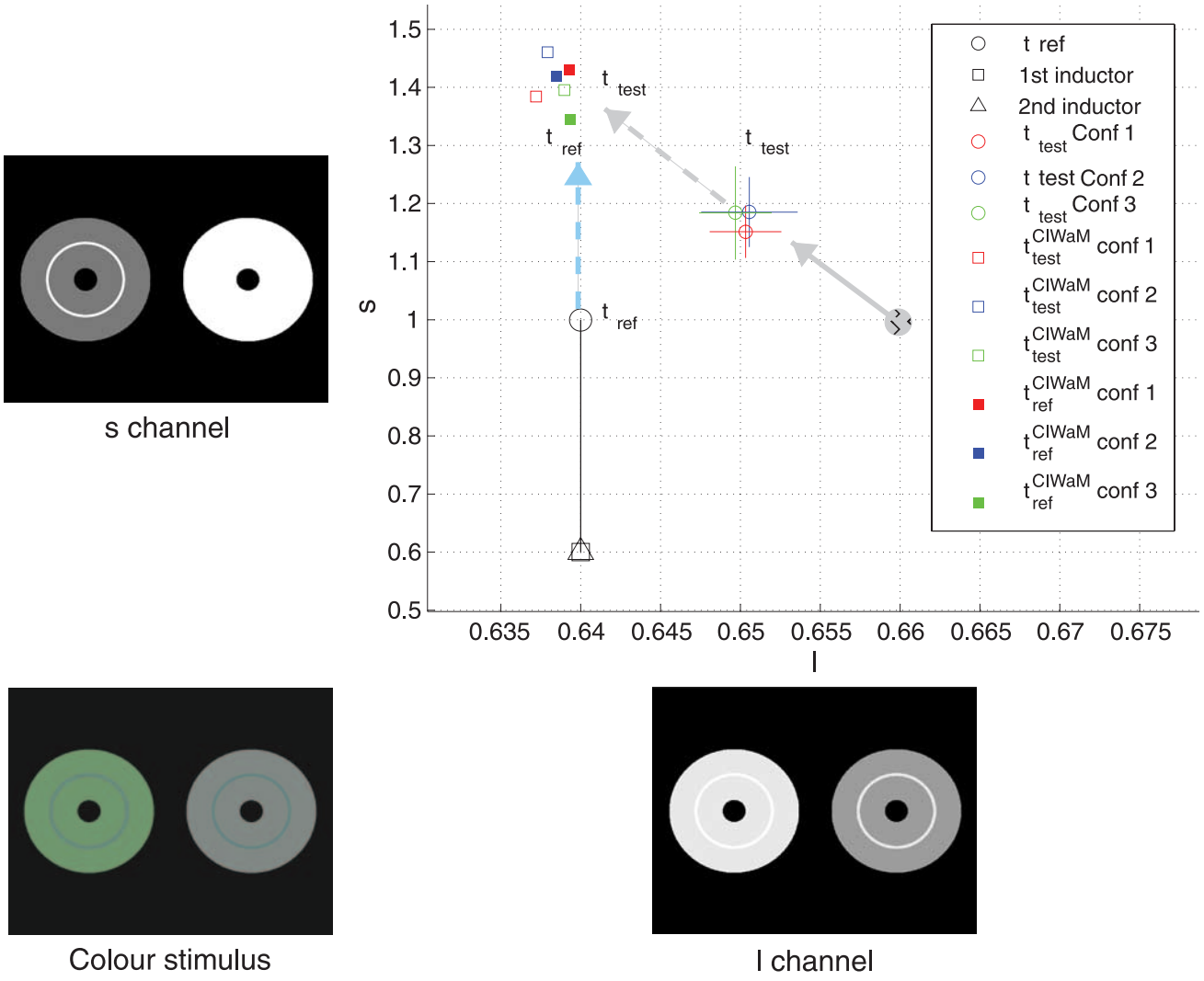

Figure 13. Experiment 2 (condition 1, all spatial configurations). Void circles with error bars represent psychophysical results (see text for explanation on vectors). Next to the chromatic axes we show the corresponding channel image. The bottom left picture shows the actual final stimulus as determined by the model.

correct. The solid line represents the best fitting (linear regression), with slopes around 0.9 and correlation coefficients $c \cong 0.95$. The mean squares of the residuals r^2 is also shown for every channel in the corresponding figure.

Figures 12 and 15 show that, despite its simplicity, CIWaM is capable of predicting both the direction and approximate magnitude of the psychophysical results. However, it is important to mention that Figures 12 and 15 conceal important systematic errors, which are conspicuous in the other result figures (e.g., where plots are systematically shorter of their target at "triangular stimuli" arrangements, e.g., Figures 8b and 9b, etc.).

At this point, it is worth pointing out that, similarly to its predecessor (BIWaM), CIWaM's parameters are not adjusted to fit individual experimental data (its algorithm only needs to consider the observer's viewing distance). All of CIWaM results were obtained by applying just the three rules based on spatial scale and surround contrast to each of the spatiochromatic color-opponent channels. We do believe that any systematic errors present at this stage will be greatly reduced once the model is thoroughly calibrated in a much larger set of experiments where the exact shape of the ECSF will be measured.

The concepts of chromatic assimilation and contrast

The results shown in Figures 8b and 9b open a new interesting question about the meaning of the words "contrast" or "assimilation" in a color context. For example, in Figure 8b there is an assimilation process along channel s since the s-component of the test ring color tends to the s value of the first inducer, i.e., the color of the test ring is shifted in the vertical direction. However, in channel l the opposite effect occurs since the l value of the test ring goes away from the l value of the first inducer, i.e., the color of the test ring is shifted

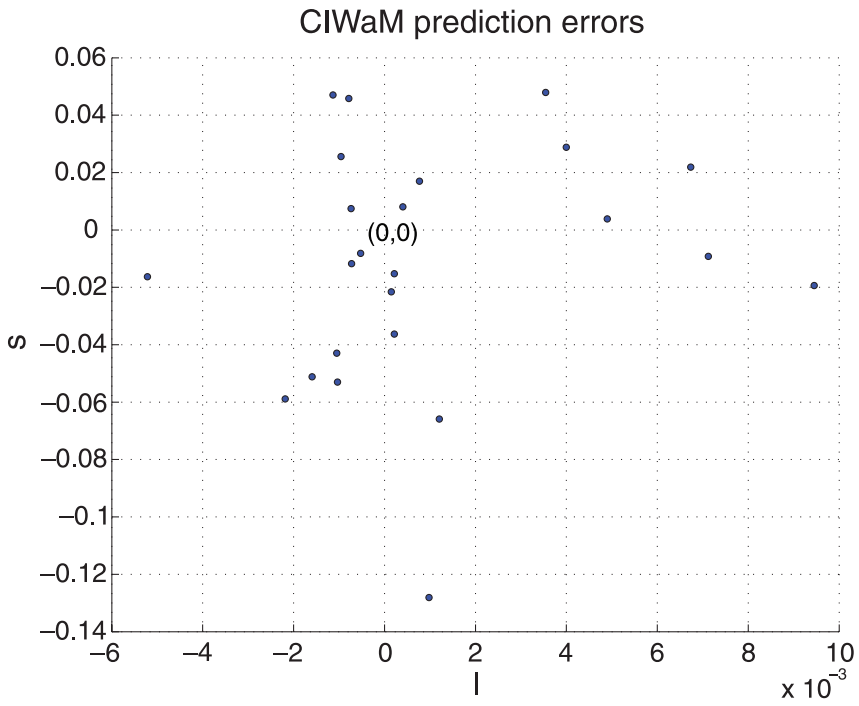

Figure 14. CIWaM errors from Analysis 2 on the *Is* chromatic plane. In the ideal case, the points would be on the (*I*, *s*) = (0, 0) location.

in the horizontal direction. As a result, the vector combination of these components does not necessarily lie in the line joining the test and the first inducer. Furthermore, we may ask what kind of effect it is, whether to call it a chromatic assimilation, a chromatic contrast, or both.

Thus, at this point we may ask whether in view of this interpretation, it makes sense to continue employing the concepts of assimilation and contrast when applied to the color domain. In fact, this general question is answered by Assumption 4.

Conclusions

Considering the good performance of our previous brightness induction model, we extended it to deal with the chromatic properties of the world. Our new simplistic model of visual chromatic induction is based on three main characteristics of visual scenes: spatial scale, spatial orientation, and center–surround chromatic contrast. We selected these not only because there is evidence that they are highly relevant to the color perception phenomena we are trying to model (Brenner et al., 2003; Brown & MacLeod, 1997; Chubb et al., 1989; Harrar & Vienot, 2005; Kinney, 1962; Monnier & Shevell, 2003; Shevell & Monnier, 2005; Shevell & Wei, 1998; Singer & D'Zmura, 1994; Walraven, 1973; Wässle & Heinrich, 1970; Wesner & Shevell, 1992) but also because there is evidence (both psychophysical and physiological) that these attributes are processed in parallel by pre-cortical and cortical semi-independent channels (De Valois et al., 1982; Legge & Foley, 1980). In our framework, we assume that chromatic induction is performed mainly on image features of similar SF (i.e., within the same multiresolution wavelet plane) and that the effect is also dependent on the contrast of the surround features (weighted against that of the central test features) at each spatial scale.

	I	*s*	ϒ
$\bar{\sigma}_{test}$	0.0037	0.0741	1.8846
$\sigma_{CIWaM-test}$	0.0034	0.0417	1.4981

Table 3. Summary of the standard deviation for all experiments and configurations. First row: mean standard deviation of the psychophysical results obtained by the observers for all the experiments and configurations. Second row: standard deviation of $\mathbf{t}_{CIWaM-test}$ (see text for details), which ideally should be zero.

	I	*s*	ϒ
$\sigma^{CIWaM}{}_{ref-test}/\bar{\sigma}^{CIWaM}{}_{test}$	0.9081	0.5634	0.7949
$\sigma_{CIWaM-test}/\bar{\sigma}_{test}$	0.9374	0.5799	0.8008

Table 4. First row: ratio between the uncertainty of CIWaM's results and the subjects', when CIWaM is applied *after* the subjects modify the test ring color (Analysis 1). Second row: ratio between the uncertainty of CIWaM's and the subjects' when CIWaM simulates a human subject (Analysis 2). In both cases, the uncertainty ratios are of the same magnitude.

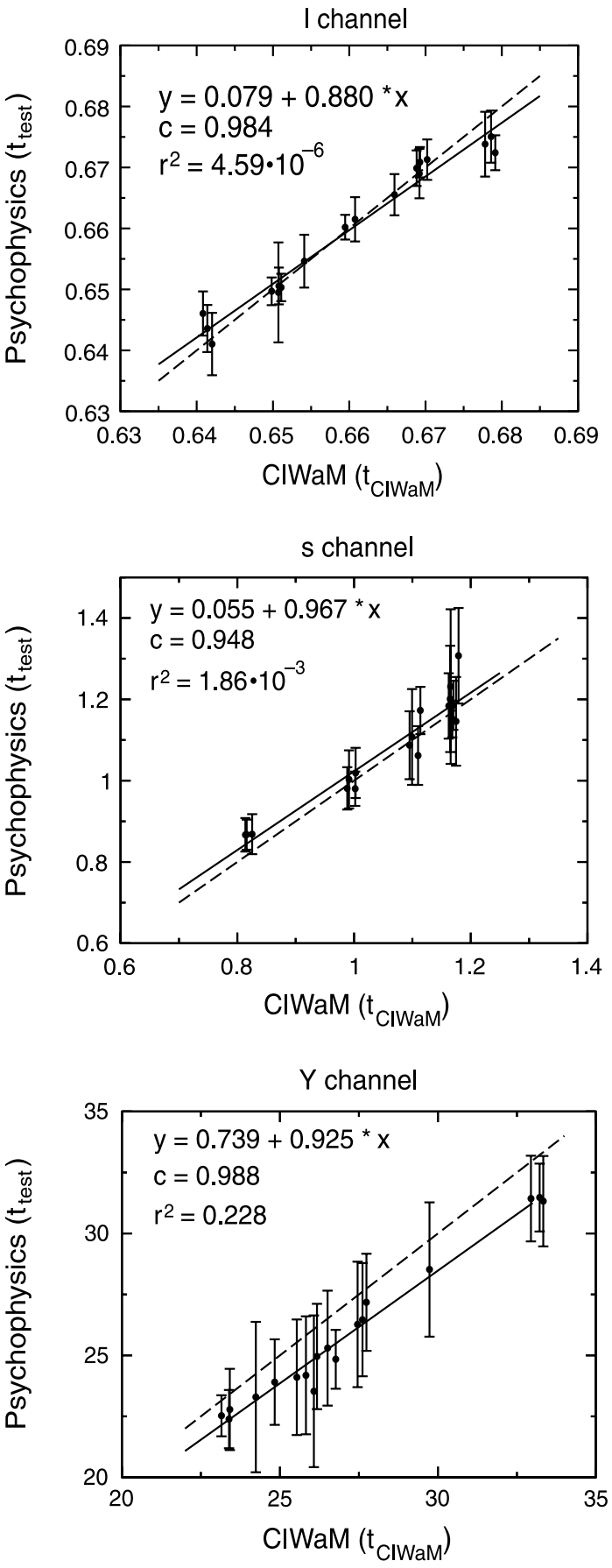

To introduce these center–surround and spatial scale effects simultaneously, we created an extended version of the CSF (the ECSF, specified in Equation 3), which modifies the way each wavelength plane interacts to produce the final image according to the center–surround contrast energy ratio. This ECSF is biologically inspired in the sense that its shape varies between low-pass (for low center–high surround contrast energy) and band-pass (for high center–low surround contrast energy) and replicates the psychophysically measured human CSF for balanced center–surround contrast energy. In other words, the human CSF is a particular case (when $r = 1$) of the ECSF.

As it happened before with the brightness version of the model (BIWaM), this rather simple set of assumptions allows for the unification of the standard concepts of chromatic assimilation and chromatic contrast in a single mathematical framework, reproducing (qualitatively in all cases, quantitatively in some) several chromatic induction effects, without the need of adjusting the model's parameters for each of them.

We believe that our most important contribution here is to show that chromatic induction effects can be modeled and reproduced using only three of the assumptions described in the Introduction section (the assumption regarding spatial orientation was not tested). A secondary contribution is the incorporation of a modified Assumption 3, which states that when the chromatic contrast of the surround features increases, chromatic assimilation increases, i.e., chromatic contrast decreases, and vice versa. This assumption is the key point that allows (under a unified mathematical formulation) the model to perform either chromatic assimilation or chromatic contrast depending on the center–surround spatial chromatic distribution and the observer's distance to the stimuli. A final contribution is to produce a model that can simultaneously replicate chromatic induction effects without the need to adjust its parameters in each particular case, in a manner consistent with the behavior of the human visual system.

From the psychophysical results, we also pose the question of whether the concepts of assimilation and contrast need to be revised for the chromatic case, since assimilation effects do not always imply that the perceived color would lay on the line determined by the test and the inducing colors in chromaticity space.

We plan in the future to concentrate on the psychophysical determination of the profile of the extended CSF. There

Figure 15. Model predictions (abscissas) against psychophysical results (ordinates) for all the chromatic conditions and spatial configurations, separated according to MacLeod–Boynton chromaticity and luminance channel. Each point represents one of the 24 runs (see Methods section) and is the mean of three observers who repeated the experiments three times each. The error bars represent standard deviations of these nine individual results, the broken line shows the diagonal of the plot, and the solid line shows the linear regression of the results. Details of the fits are also shown.

is also a need for exploring the behavior of the model when presented with other (more complex) visual contrast phenomena, different colors, etc.

CIWaM can be tried online at http://www.cat.uab.cat/Software/perception/CIWaM/.

Appendix A

Psychophysical results

Results of all our psychophysical experiments are presented in two tables (for Experiments 1 and 2). More details about particular conditions, configurations, and experimental settings in general can be found in the Methods section and in Table 1.

Acknowledgments

C. Alejandro Parraga was funded by the "Ramon y Cajal" program of the Spanish MEC (Ministry of Science)-Ref. RYC-2007-00484. This work has been partially supported by Project TIN2007-64577 and Project Consolider-Ingenio 2010-CSD2007-00018 of the Spanish MEC (Ministry of Science). The authors wish to thank Naila Murray for her insightful comments.

Commercial relationships: none.
Corresponding author: Xavier Otazu.
Email: xotazu@cvc.uab.es.
Address: CVC Edifici 'O' UAB Campus (Bellaterra), 08193 Barcelona, Spain.

References

Blakemore, C., & Campbell, F. W. (1969). On the existence of neurons in the human visual system selectively sensitive to the orientation and size of retinal images. *The Journal of Physiology, 203,* 237–260.

Blakeslee, B., & McCourt, M. E. (1999). A multiscale spatial filtering account of the White effect, simultaneous brightness contrast and grating induction. *Vision Research, 39,* 4361–4377.

Boynton, R. M. (1986). A system of photometry and colorimetry based on cone excitations. *Color Research and Application, 11,* 244–252.

Boynton, R. M. (1996). Frederic Ives Medal paper. History and current status of a physiologically based system of photometry and colorimetry. *Journal of the Optical Society of America A, 13,* 1609–1621.

Brainard, D. H. (1997). The psychophysics toolbox. *Spatial Vision, 10,* 433–436.

Brenner, E., & Cornelissen, F. W. (1998). When is a background equivalent? Sparse chromatic context revisited. *Vision Research, 38,* 1789–1793.

Brenner, E., Ruiz, J. S., Herraiz, E. M., Cornelissen, F. W., & Smeets, J. B. (2003). Chromatic induction and the layout of colours within a complex scene. *Vision Research, 43,* 1413–1421.

Bressan, P. (2001). Explaining lightness illusions. *Perception, 30,* 1031–1046.

Brown, R. O., & MacLeod, D. I. A. (1997). Color appearance depends on the variance of surround colors. *Current Biology, 7,* 844–849.

Cannon, M. W., & Fullenkamp, S. C. (1991). Spatial interactions in apparent contrast: Inhibitory effects among grating patterns of different spatial frequencies, spatial positions and orientations. *Vision Research, 31,* 1985–1998.

Chevreul, M. E. (1839). *De la loi du contraste simultané des couleurs*. Paris: Pitois-Levrault.

Chichilnisky, E. J., & Wandell, B. A. (1995). Photoreceptor sensitivity changes explain color appearance shifts induced by large uniform backgrounds in dichoptic matching. *Vision Research, 35,* 239–254.

Chubb, C., Sperling, G., & Solomon, J. A. (1989). Texture interactions determine perceived contrast. *Proceedings of the National Academy of Sciences of the United States of America, 86,* 9631–9635.

da Vinci, L. (1651/2005). *A treatise on painting* (J. F. Rigaud, Trans.). Mineola, NY: Dover.

Derrington, A. M., Krauskopf, J., & Lennie, P. (1984). Chromatic mechanisms in lateral geniculate nucleus of macaque. *The Journal of Physiology, 357,* 241–265.

De Valois, R. L., Albrecht, D. G., & Thorell, L. (1982). Spatial-frequency selectivity of cells in macaque visual cortex. *Vision Research, 22,* 545–559.

D'Zmura, M. (1998). *Color contrast gain control*. Berlin, Germany: Walter de Gruyter.

D'Zmura, M., & Singer, B. (1999). Contrast gain control. In K. R. Gegenfurtner & L. T. Sharpe (Eds.), *Color vision: From genes to perception* (2001 ed., pp. 369–385). Cambridge, UK: Cambridge University Press.

Ejima, Y., & Takahashi, S. (1985). Apparent contrast of a sinusoidal grating in the simultaneous presence of peripheral gratings. *Vision Research, 25,* 1223–1232.

Ellemberg, D., Wilkinson, F., Wilson, H. R., & Arsenault, A. S. (1998). Apparent contrast and spatial frequency

of local texture elements. *Journal of Optical Society of America A, Optics, Image Science, and Vision, 15,* 1733–1739.

Fach, C., & Sharpe, L. T. (1986). Assimilative hue shifts in color gratings depend on bar width. *Perception & Psychophysics, 40,* 412–418.

Fairchild, M. D. (1998). *Color appearance models*. Reading, MA; Harlow: Addison-Wesley.

Gilchrist, A. L. (2006). *Seeing black and white*. Oxford, UK: Oxford University Press.

Graham, N., & Nachmias, J. (1971). Detection of grating patterns containing two spatial frequencies: A comparison of single-channel and multiple-channels models. *Vision Research, 11,* 251–259.

Harrar, M., & Vienot, F. (2005). Regulation of chromatic induction by neighboring images. *Journal of the Optical Society of America A, 22,* 2197–2206.

Heeger, D. J. (1992). Normalization of cell responses in cat striate cortex. *Visual Neuroscience, 9,* 181–197.

Helmholtz, H. v. (1867). *Handbuch der physiologischen optik*. Leipzig, Germany: Voss.

Jameson, D., & Hurvich, L. M. (1961). Opponent chromatic induction: Experimental evaluation and theoretical account. *Journal of the Optical Society of America, 51,* 46–53.

Kingdom, F. A. A. (1999). Old wine in new bottles? Some thoughts on Logvinenko's "Lightness induction revisited". *Perception, 28,* 929–934.

Kinney, J. A. S. (1962). Factors affecting induced color. *Vision Research, 2,* 503–525.

Kirschmann, A. (1890). *Ueber dis quantitativen verhältnisse des simultanen helligkeits- und farben-contrastes*. Leipzig, Germany: W. Engelmann.

Klein, S., Stromeyer, C. F., & Ganz, L. (1974). The simultaneous spatial frequency shift: A dissociation between the detection and perception of gratings. *Vision Research, 14,* 1421–1432.

Legge, G. E., & Foley, J. M. (1980). Contrast masking in human vision. *Journal of the Optical Society of America, 70,* 1456–1471.

Lucassen, M., & Walraven, J. (1993). Quantifying color constancy—Evidence for non-linear processing of cone-specific contrast. *Vision Research, 33,* 739–757.

MacKay, D. M. (1973). Lateral interaction between neural channels sensitive to texture density? *Nature, 245,* 159–161.

Monnier, P. (2008). Standard definitions of chromatic induction fail to describe induction with S-cone patterned backgrounds. *Vision Research, 48,* 2708–2714.

Monnier, P., & Shevell, S. K. (2003). Large shifts in color appearance from patterned chromatic backgrounds. *Nature Neuroscience, 6,* 801–802.

Monnier, P., & Shevell, S. K. (2004). Chromatic induction from S-cone patterns. *Vision Research, 44,* 849–856.

Mullen, K. T. (1985). The contrast sensitivity of human color vision to red–green and blue–yellow chromatic gratings. *The Journal of Physiology, 359,* 381–400.

Nachmias, J., & Sansbury, R. V. (1974). Grating contrast discrimination may be better than detection. *Vision Research, 14,* 1039–1042.

Otazu, X., Vanrell, M., & Párraga, C. A. (2008a). Colour induction effects are modelled by a low-level multiresolution wavelet framework. *Perception, 37,* 107.

Otazu, X., Vanrell, M., & Párraga, C. A. (2008b). Multiresolution wavelet framework models brightness induction effects. *Vision Research, 48,* 733–751.

Pessoa, L. (1996). Mach bands: How many models are possible? Recent experimental findings and modeling attempts. *Vision Research, 36,* 3205–3227.

Shevell, S. K., & Monnier, P. (2005). Color shifts from S-cone patterned backgrounds: Contrast sensitivity and spatial frequency selectivity. *Vision Research, 45,* 1147–1154.

Shevell, S. K., & Monnier, P. (2006). Color shifts induced by S-cone patterns are mediated by a neural representation driven by multiple cone types. *Visual Neuroscience, 23,* 567–571.

Shevell, S. K., & Wei, J. P. (1998). Chromatic induction: Border contrast or adaptation to surrounding light? *Vision Research, 38,* 1561–1566.

Simpson, W. A., & McFadden, S. M. (2005). Spatial frequency channels derived from individual differences. *Vision Research, 45,* 2723–2727.

Singer, B., & D'Zmura, M. (1994). Color contrast induction. *Vision Research, 34,* 3111–3126.

Singer, B., & D'Zmura, M. (1995). Contrast gain control: A bilinear model for chromatic selectivity. *Journal of the Optical Society of America A, Optics, Image Science, and Vision, 12,* 667–685.

Smith, V. C., Jin, P. Q., & Pokorny, J. (2001). The role of spatial frequency in color induction. *Vision Research, 41,* 1007–1021.

Smith, V. C., & Pokorny, J. (1975). Spectral sensitivity of the foveal cone photopigments between 400 and 500 nm. *Vision Research, 15,* 161–171.

Solomon, J. A., Sperling, G., & Chubb, C. (1993). The lateral inhibition of perceived contrast is indifferent to on-center/off-center segregation, but specific to orientation. *Vision Research, 33,* 2671–2683.

Sperling, G. (1989). Three stages and two systems of visual processing. *Spatial Vision, 4,* 183–207.

Spitzer, H., & Barkan, Y. (2005). Computational adaptation model and its predictions for color induction

of first and second orders. *Vision Research, 45,* 3323–3342.

Valberg, A., & Lange-Malecki, B. (1990). "Colour constancy" in Mondrian patterns: A partial cancellation of physical chromaticity shifts by simultaneous contrast. *Vision Research, 30,* 371–380.

Wachtler, T., Albright, T. D., & Sejnowski, T. J. (2001). Nonlocal interactions in color perception: Nonlinear processing of chromatic signals from remote inducers. *Vision Research, 41,* 1535–1546.

Walker, J. T. (1978). Brightness enhancement and the Talbot level in stationary gratings. *Perception & Psychophysics, 23,* 356–359.

Walraven, J. (1973). Spatial characteristics of chromatic induction: The segregation of lateral effects from straylight artefacts. *Vision Research, 13,* 1739–1753.

Ware, C., & Cowan, W. B. (1982). Changes in perceived color due to chromatic interactions. *Vision Research, 22,* 1353–1362.

Wässle, H., & Heinrich, F. (1970). Untersuchungen zum helligkeitskontrast. *Vision Research, 10,* 361–373.

Werner, A. (2003). The spatial tuning of chromatic adaptation. *Vision Research, 43,* 1611–1623.

Werner, J. S., & Walraven, J. (1982). Effect of chromatic adaptation on the achromatic locus: The role of contrast, luminance and background color. *Vision Research, 22,* 929–943.

Wesner, M. F., & Shevell, S. K. (1992). Color perception within a chromatic context: Changes in red/green equilibria caused by noncontiguous light. *Vision Research, 32,* 1623–1634.

Wilson, H. R., McFarlane, D. K., & Phillips, G. C. (1983). Spatial frequency tuning of orientation selective units estimated by oblique masking. *Vision Research, 23,* 873–882.

Xing, J., & Heeger, D. J. (2001). Measurement and modeling of center–surround suppression and enhancement. *Vision Research, 41,* 571–583.

Yu, C., Klein, S. A., & Levi, D. M. (2001). Surround modulation of perceived contrast and the role of brightness induction. *Journal of Vision, 1*(1):3, 18–31, http://www.journalofvision.org/content/1/1/3, doi:10.1167/1.1.3. [PubMed] [Article]

Yu, C., Klein, S. A., & Levi, D. M. (2002). Facilitation of contrast detection by cross-oriented surround stimuli and its psychophysical mechanisms. *Journal of Vision, 2*(3):4, 243–255, http://www.journalofvision.org/content/2/3/4, doi:10.1167/2.3.4. [PubMed] [Article]

Yu, C., Klein, S. A., & Levi, D. M. (2003). Cross- and iso-oriented surrounds modulate the contrast response function: The effect of surround contrast. *Journal of Vision, 3*(8):1, 527–540, http://www.journalofvision.org/content/3/8/1, doi:10.1167/3.8.1. [PubMed] [Article]